J. Fluid Mech. (1992), *vol.* 241, *pp.* 75–108
Printed in Great Britain

Bursts and the law of the wall in turbulent boundary layers

By J. F. MORRISON, C. S. SUBRAMANIAN† AND P. BRADSHAW‡
Department of Aeronautics, Imperial College, Prince Consort Road, London, SW7 2BY, UK

(Received 7 March 1990 and in revised form 10 January 1992)

The bursting mechanism in two different high-Reynolds-number boundary layers has been analysed by means of conditional sampling. One boundary layer develops on a smooth, flat plate in zero pressure gradient; the other, also in zero pressure gradient, is perturbed by a rough-to-smooth change in surface roughness and the new internal layer has not yet recovered to the local equilibrium condition at the measurement station. Sampling on the instantaneous uv signal in the logarithmic region confirms the presence of two related structures, 'ejections' and 'sweeps' which, in the smooth-wall layer, appear to be responsible for most of the turbulent energy production, and to effect virtually all that part of the spectral energy transfer that is universal. Ejections show features similar to those of Falco's 'typical eddies' while sweeps appear to be inverted ejections moving down towards the wall. The inertial structures associated with ejections show attributes of the true universal motion (Townsend's 'attached' eddies) of the inner layer and these are therefore identified as 'bursts'. In the outer layer, these become 'detached' from the wall. The large-scale structures associated with sweeps also appear to be 'detached' eddies ('splats'), but these induce low-wave-number inactive motion near the wall and this is not universal even though the sweep itself is. Neither ejections nor sweeps detected in the rough-to-smooth layer are near a condition of energy equilibrium. The relation of ejections and sweeps to the law of the wall and other accepted laws is discussed.

1. Introduction

According to the 'law of the wall' (Coles 1955, 1956), the mean velocity in the inner layer of a turbulent wall flow ($y/\delta < 0.2$) scales on the friction velocity, $u_\tau = (T_w/\rho)^{\frac{1}{2}}$, where T_w is the wall shear stress, the distance from the surface, y and the kinematic viscosity, ν. Outside the viscous sublayer and buffer layer ($y^* = yu_\tau/\nu > 30$), the motion scales on u_τ and y only: application of this scaling to the turbulent energy equation, leads to the 'local equilibrium' approximation, production = dissipation (Townsend 1961). (Townsend also discusses an extension of the analysis, in which the local value of $(T/\rho)^{\frac{1}{2}} \simeq (-\overline{uv})^{\frac{1}{2}}$ is used instead of u_τ where T varies with y). U_i, u_i $(i = 1, 2, 3)$ are the mean and fluctuating components of velocity (U, u) in x-(streamwise) direction; V, v in the y-direction (normal to the wall) and W, w in the z-(spanwise) direction.

† Present address: Mechanical and Aerospace Engineering Department, Florida Institute of Technology, Melbourne, FL 32901-6988, USA.
‡ Present address: Mechanical Engineering Department, Stanford University, Stanford, CA 94305-3030, USA.

It is well known that most of the turbulent shear stress in the inner layer, and therefore most of the production of turbulent energy, occurs in 'ejections' – short regions of intense turbulent activity with velocity fluctuations $u < 0$, $v > 0$. The remainder occurs mainly in 'sweeps' (Corino & Brodkey 1969), $u > 0$, $v < 0$ whose relationship with ejections is close but not simple (Offen & Kline 1974, 1975). The word 'burst' is sometimes used for 'ejection': here we call the complete sequence of outward moving fluid a 'burst' (Kim, Kline & Reynolds 1971) although, as a consequence of the present results, we attempt a more rigorous definition in §5. The interaction of the inner and outer layers is dominated by the transport of energy, momentum and vorticity that is effected by ejections (Kline *et al.* 1967) and this interaction in turn determines u_τ, a universal velocity scale for the shear-stress-bearing motion of both layers.

The initiation of bursts in and just above the sublayer is not studied here: however, in a previous paper (Morrison & Bradshaw 1989), we examined the role of wall shear stress fluctuations during ejections and sweeps and the substantive results are used here. The aim of the present paper is to examine the related question of the relationship between ejections, sweeps and the accepted laws for the boundary layer.

The law of the wall is incorporated, in some form, in all Reynolds-averaged models for turbulent stresses. It is, of course, a first approximation: the observation that the u- and w-component turbulent intensities do not scale on u_τ and y was explained by Townsend as the influence of the outer-layer large-eddy structure on the equilibrium layer. This 'inactive' motion is of low wavenumber compared to the universal inner-layer motion and is therefore not likely to interact with it. Also, being largely confined to the (x,z)-plane with $v \simeq 0$, it does not contribute to the shear-stress, $-\rho\overline{uv}$, in the inner layer and therefore is not involved in the extraction of energy from the mean flow there nor the transfer of energy to the smaller eddies. A more detailed understanding of inner-layer motion is needed for difficult cases like flow near separation, or for the formulation of simplified wall boundary conditions for 'large-eddy' simulations of turbulent flow. In the latter, large-scale eddies are computed as solutions of the time-dependent Navier–Stokes equations, but small-scale eddies are modelled throughout the flow, the model being most critical in the sublayer and buffer layer where all the eddies are 'small'.

Most previous studies have considered only boundary layers or duct flows on smooth surfaces. The present work explores the burst structure of two high-Reynolds-number boundary layers both in zero pressure gradient. One is a smooth-wall layer; the other initially develops over a rough surface and then passes onto a smooth surface. In the 'rough-to-smooth' layer, the value of u_τ at the smooth-wall measurement station is approximately the same as that in the smooth-wall layer, so that the viscous lengthscale, ν/u_τ, is much the same. However, the ratio of typical outer-layer turbulent intensity to inner-layer intensity in the smooth part of the rough-to-smooth layer is approximately double that in the smooth-wall layer, therefore permitting the study of an inner layer in which the inactive motion is particularly intense. The underlying philosophy of these experiments is the same as Clauser's (1956) 'black-box' analogy in which a self-preserving shear layer is suddenly perturbed and its behaviour observed as it asymptotes to a new self-preserving state.

The 'VITA+LEVEL' conditional-sampling scheme of Morrison, Tsai & Bradshaw (1989) is used to study the shear-stress-bearing motion of both boundary layers. Briefly, the purpose of conditionally sampling a time-dependent signal, $f(t)$, is to generate an on–off signal, $c(t)$, which is equal to one at times when $f(t)$ satisfies some

arbitrary criterion as being 'interesting' and zero at other times. The criterion relies on the prejudices of the user and a very simple one would be $f(t) > F$ where F is the pre-chosen threshold value. The 'contribution' to the conventional mean is $\overline{c(t)f(t)}$ and the 'event average' is $\overline{c(t)f(t)}/\overline{c(t)} = \widetilde{f(t)}$ (notation from Kovasznay, Kibens & Blackwelder 1970). Computer recognition of ejections and sweeps is notoriously difficult and the choice of sampling signal and thresholds is crucial. Here, the VITA + LEVEL algorithm is applied to the instantaneous uv signature (because calculation methods require satisfactory modelling of $\overline{uv}$ in particular) using thresholds that are universal multiples of the local value of $-\overline{uv}$. See Morrison *et al.* (1989). Chen & Bradshaw (1990) have also shown that the scheme gives an almost one-to-one correspondence with visually identified peaks in the instantaneous contours of uv in the (x, z)-plane from simulated-channel-flow data. In spite of its apparent success, the final test of such a scheme is that the hypothesized structures should be consistent with the logarithmic and defect laws, at least to a first approximation. The Reynolds number of both boundary layers is above 5000 so that they are both virtually unaffected by the viscous superlayer (Murlis, Tsai & Bradshaw 1982) and the defect law can properly be expected to hold: any structure that obeys viscous scaling and is at $y^* > 30$ cannot contribute directly to $\overline{uv}$. Conversely, any structure that obeys outer layer scaling (u_τ, δ) cannot, as we have seen, contribute directly to $\overline{uv}$ in the inner layer if the law of the wall is to hold. In the rough-to-smooth layer, the log law is apparently obeyed while the event statistics indicate significant advection and diffusion of turbulent energy that violate the local equilibrium approximation.

Bursting predominates in the buffer region ($10 < y^* < 30$) and its relevance to the present measurements made in the logarithmic region (and further from the wall) lies in the observation, made by Offen & Kline (1974), that each 'lift-up' of a sublayer 'streak' is associated with a disturbance in the logarithmic region. Offen & Kline's study indicated the possibility that bursts and sweeps are related in a cyclic fashion: the interaction of bursts with fluid in the logarithmic region produces sweeps which influence the generation of bursts further downstream. They also observed that a sweep was related to a region of high shear in the logarithmic region produced by what appeared to be either a spanwise vortex or an upward-tilted streamwise vortex (i.e. part of a 'hairpin' vortex). The effect of bursts on the motion in the logarithmic region was to produce another sweep linked to the burst by the vortex-like structure. Offen & Kline (1975) suggested that the formation of a spanwise vortex near the wall results from the relative motion between a burst and the replacement fluid required by continuity. This would suggest that a locally-adverse pressure gradient either produces, or is produced by, the observed lift-up: the role of pressure fluctuations in bursting is examined in a companion paper by Morrison, Subramanian & Bradshaw (1992).

Falco (1977) showed that 'typical eddies' produce most of the shear stress in the outer layer (and therefore also in the inner layer). Subsequently, Falco (1979, 1980) showed that 'pockets' or large-eddy 'footprints', formed by the convection of typical eddies towards the wall by the downstream face of the large-scale structure, are responsible for the initiation of bursting just above the sublayer in a way that is reminiscent of the burst-sweep cycle proposed by Offen & Kline. More recently, several workers (see the review by Hunt 1988) with the aid of channel simulation data, have been able to trace spatially compact, organized structures for a long streamwise extent, suggesting that they diffuse slowly. Falco (1974) observed typical eddies that persisted for streamwise distances of up to 15δ.

Theodorsen (1952) first postulated that the hairpin or 'horseshoe' vortex is the dominant flow mechanism in turbulent shear flows. He suggested that the primary hairpins are aligned in the direction of maximum mean strain rate (the principal axis) at 45° to the mean flow direction so that turbulent energy production is maximized. Until fairly recently, these ideas had only qualitative support: for example, the wall-pressure/spanwise velocity ($\overline{pw}$) correlations of Willmarth & Tu (1967) who hypothesized a pattern of 'swept-back' vorticity near the wall. The 'double-cone' eddy of Townsend (1976) can also be thought of as a hairpin vortex without the spanwise connecting loop. More recently, channel simulation data (Moin & Kim 1985; Kim & Moin 1986) and simulations of homogeneous turbulence (Rogers & Moin 1987), all at low Reynolds numbers, tend to support Theodorsen's theory. However, Guezennec, Piomelli & Kim (1987) and Robinson (1990) have shown that complete, near-symmetrical horseshoes are rare: more common are j-shaped ('arch-like') vortices, in effect a horseshoe with one leg replaced by more diffuse vorticity.

Direct support for the presence of horseshoe vortices at low to relatively high Reynolds numbers comes from the flow-visualization experiments of Head & Bandyopadhyay (1981) who observed horseshoes inclined at 45°. At their highest Reynolds number based on momentum thickness, $Re_\theta = 9400$, they noted that there were noticeably fewer hairpins in the outer layer and that there was no conclusive evidence to link near-wall eruptions with the inclined vortex loops in the outer layer. If one accepts the view that Falco's typical eddies are a section in the (x, y)-plane through the tip of a horseshoe, then Falco's flow visualization experiments endorse the belief that horseshoes or typical eddies exist in both the inner and outer layers for $1000 < Re_\theta < 10000$ and that their dimensions are strongly Reynolds-number dependent when non-dimensionalized by the boundary-layer thickness, δ, but less so when non-dimensionalized by ν/u_τ. These Reynolds-number variations are consistent with the view put forward by Murlis *et al.* (1982), that at low Reynolds number, large eddies or horseshoes and typical eddies (a section through the horseshoe tip) accomplish a similar degree of momentum transport, while at high Reynolds numbers, the contribution by the large eddies increases and that of typical eddies decreases. As the Reynolds number increases, vortex stretching reduces the diameter of the horseshoe while increasing the overall streamwise length of the vortex, although Kim *et al.* (1971) have suggested that only the legs of the hairpin, and not the tip, are stretched.

Moin, Leonard & Kim (1986) have also investigated Falco's (1983; see also Chu & Falco 1988) claim of the appearance of vortex rings (which Falco calls typical eddies) in the outer layer by calculating the Biot–Savart induction caused by a parabolic vortex subject to a shear and the impermeability constraint independently. The vortex was observed to pinch off to form a ring. They also simulated a vortex sheet subjected to an upward perturbation (as in an ejection) in a channel flow. Their calculations show the evolution of a horseshoe vortex, the tip of which again pinches off into a vortex ring. We estimate their value of Re_θ to be about 800 and pinching occurs at a time, t, after the initiation of the calculation corresponding to $tU_c/(\nu/u_\tau) \approx 7500$ or $tU_c/\delta \approx 42$ where U_c is the channel centreline velocity. This time is roughly four times the expected large-eddy lifetime so that even at this low Reynolds number, pinching could be expected to be a relatively rare phenomenon. Furthermore, as Moin *et al.* indicate, the actual closing of the vortex ring involves significant viscous diffusion which would be dominated by inertial effects of high Reynolds numbers. But Head & Bandyopadhyay (1981) have pointed out that pairing of horseshoe vortices in the wall region could considerably increase the range

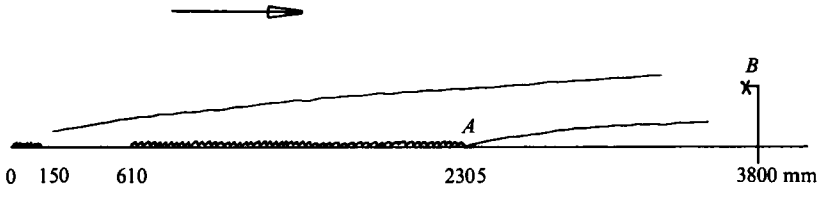

	Rough-to-smooth		Smooth
	A	*B*	
u_τ	2.50	1.05	1.09 ms^{-1}
U_e	33.5	33.5	32.8 ms^{-1}
δ_{995}	96.9	119.0	68.2 mm
C_f	0.0111	0.00197	0.00222
δ^*	19.9	18.7	8.93 mm
θ	12.8	14.1	6.93 mm
H	1.56	1.32	1.29
Re_θ	2.73×10^4	3.00×10^4	1.45×10^4

FIGURE 1. Schematic diagram of rough-to-smooth flow and table of integral parameters.

of eddy sizes: this effect is not included in Moin *et al.*'s simulations so that our estimates could be regarded as unduly pessimistic. Yet Robinson (1991) shows that horseshoe vortices are so asymmetric that it is difficult to see how the symmetrical phenomenon of pinch-off could occur. The possible similarity between ejections and sweeps and Falco's typical eddies is discussed in §3.

2. Description of the boundary layers

Details of the zero-pressure-gradient smooth-wall boundary layer can be found in any standard text (e.g. Ligrani 1989). Our measurements of conventionally averaged statistics, even third- and fourth-order velocity products, are closely self-preserving and agree well with those of other authors e.g. Klebanoff (1954); Andreopoulos (1978). The experimental procedures, and data acquisition and reduction techniques are all described by Morrison *et al.* (1989) except those for the surface-mounted hot wire which are described by Morrison & Bradshaw (1989). The design and use of the four-wire array used to make low-wave-number measurements of spanwise components of fluctuating strain rate (s_{12}) and vorticity (ω_3) are described by Subramanian, Kandola & Bradshaw (1985).

Figure 1 shows the development of the rough-to-smooth layer and the position of the measurement station, B relative to the change of surface ('step') at A. The boundary layer develops on the smooth wall over an additional fetch of 1495 mm. The roughness is an array of uniformly distributed 13 mm cubes. The integral parameters just upstream of the step were estimated rather than measured directly; those at B were measured. θ_A is deduced from θ_B by integrating the momentum integral equation between A and B using measured values of skin-friction coefficient, C_f. At A, the wake profile parameter, Π, was taken to be 0.6 from which values of displacement thickness, δ^* and δ can be deduced using the wake function of Coles & Hirst (1968). $C_{f,A}$ was taken to be $(2\theta/x)_A$, where x is measured from the beginning of the roughness. Note that the deduced value of θ_A assumes the validity of the log law implicit in the measurements of C_f between A and B made with a Preston tube.

Townsend (1966) describes the boundary layer following a step change in surface roughness as being in 'moving equilibrium', that is, in a state which is locally self-

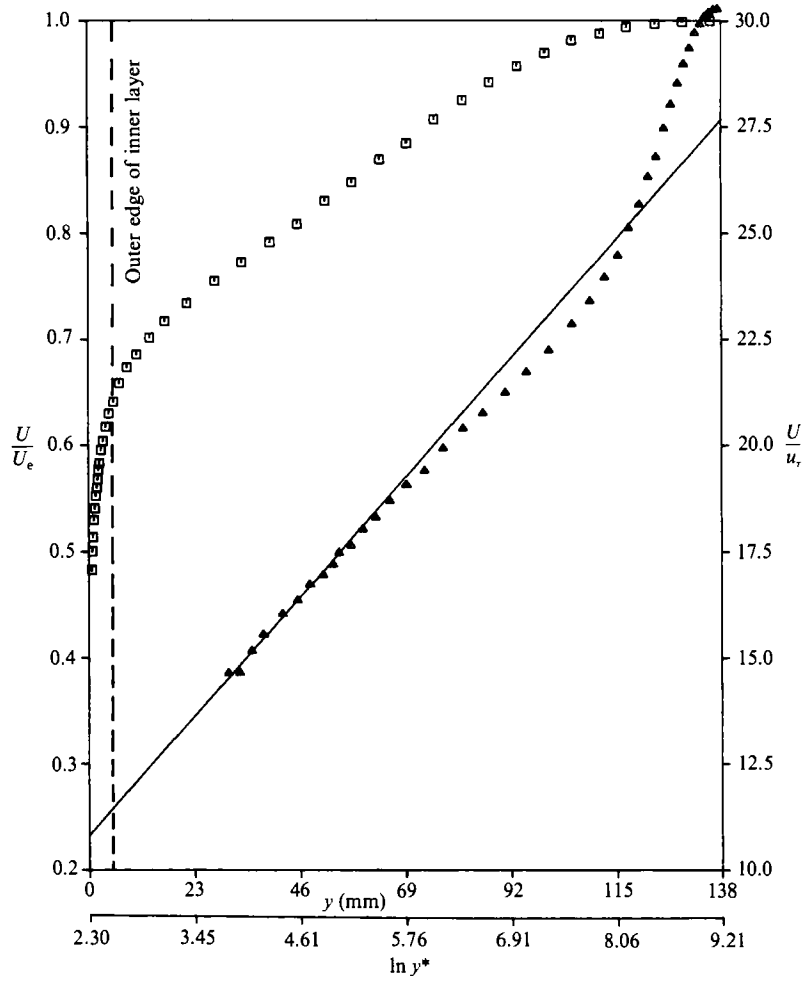

FIGURE 2. Mean velocity profile and Clauser plot of rough-to-smooth boundary layer at B. ——, $U/u_\tau = (1/\kappa)\ln y^* + C$. $\kappa = 0.41$, $C = 5.2$.

preserving but where lengthscales and velocity scales change slowly with x_s, the streamwise fetch measured downstream from the step. His analysis assumes not only that the ratio of x_s to the internal layer thickness is large but also that there is a near-wall region which is in local equilibrium. The measurements of Antonia & Luxton (1972) following a rough-to-smooth step show that significant advection and diffusion near the wall invalidate the local-equilibrium approximation, which explains why their distributions of mean velocity and shear stress in the inner layer are not self-preserving, even in the last measurement station, $x_s = 16.1\,\delta^A_{995}$.

The best measure of the strength of the surface change is indicated by the ratio of wall lengthscales, namely

$$M_{RS} = \ln(Z_{0A}/Z_{0B}), \tag{2.1}$$

where Z_{0A} and Z_{0B} are the wall lengthscales defined by the logarithmic law:

$$\frac{U}{u_\tau} = \frac{1}{\kappa}\ln(y/Z_0) \tag{2.2}$$

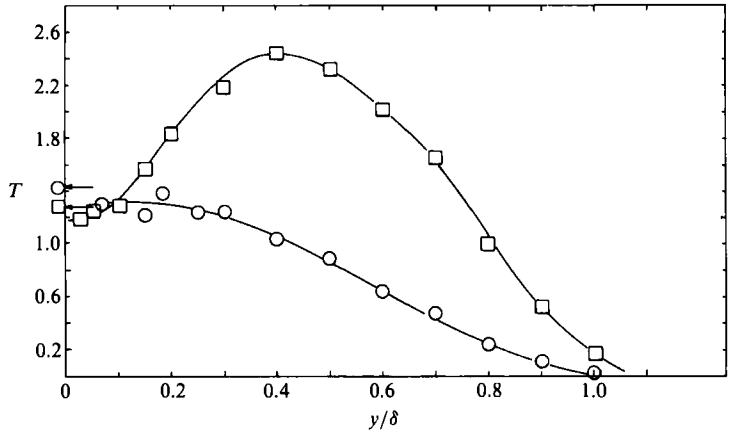

FIGURE 3. Shear stress profiles, $T = -\rho\overline{uv}$. ○, smooth; □, rough-to-smooth. ←, wall shear stress (Preston tube).

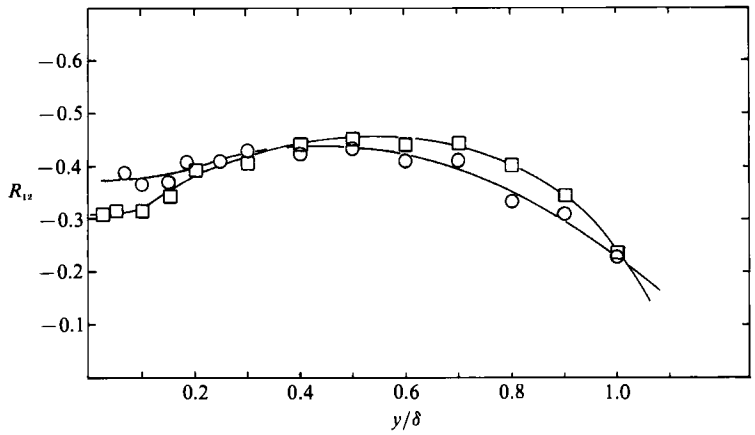

FIGURE 4. Shear correlation coefficient, R_{12}. Symbols as in figure 3.

for rough and smooth walls respectively, where κ is the von Kármán constant. Our value of M_{RS} is 4.25, evaluated at $x_s = 15.4\,\delta^A_{995}$: Antonia & Luxton's value at their last measurement position is 5.8 so that our experiment represents a somewhat weaker perturbation. Schofield (1981) has made an extensive analysis of data taken in both rough-to-smooth and smooth-to-rough configurations and suggest that for the former, departures from true wall similarity will be small only for $x_s > 20\,\delta^A_{995}$. This suggests that our data do not conform to Townsend's moving-equilibrium condition and that in the inner layer of the internal layer, advection and y-wise diffusion of energy are still significant. In fact, figure 2 indicates that the thickness of the inner layer is roughly 5 mm so that only one or possibly two points of the hot-wire traverses lie within the approximate local-equilibrium region. A complete energy balance for this layer is given in a companion paper by Morrison & Bradshaw (1992) who examine the y-wise diffusion of energy and heat when the internal layer is slightly heated.

Figures 3 and 4 show the shear-stress profiles and shear correlation coefficients for both boundary layers as an illustration of the perturbation of the rough-to-smooth

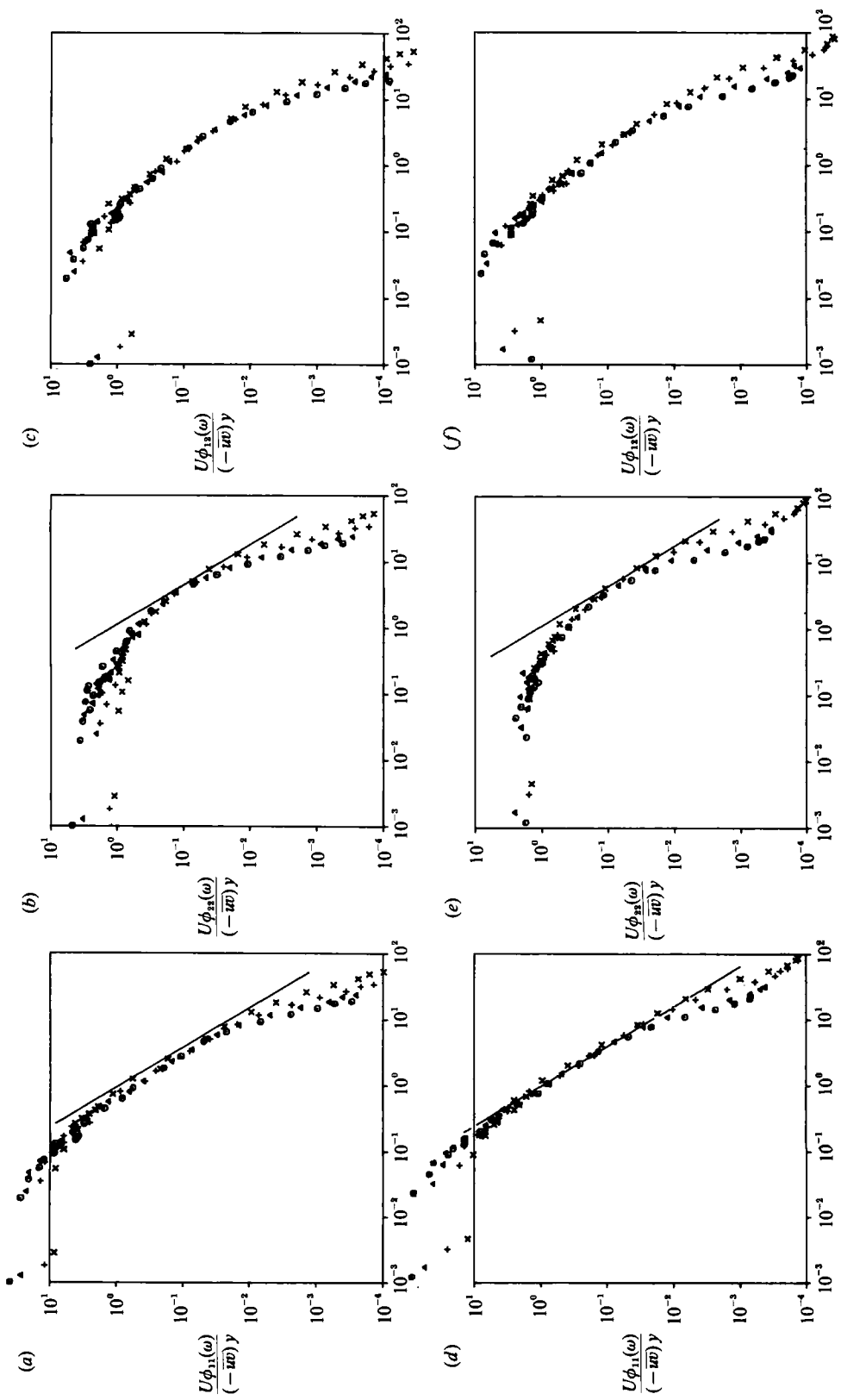

FIGURE 5. Inner-layer frequency spectra: smooth-wall layer; (*a*) $U\phi_{11}(\omega)/(-\overline{uv}\,y)$ *vs.* $\omega y/U$; (*b*) ϕ_{22}; (*c*) ϕ_{12}. Rough-to-smooth layer; (*d*) ϕ_{11}; (*e*) ϕ_{22}; (*f*) ϕ_{12}. ——, equation (2.3). Smooth: ⊙, $y/\delta = 0.051$; △, 0.069; +, 0.103; ×, 0.170. Rough-to-smooth: ⊙, 0.033; △, 0.05; +, 0.10; ×, 0.15.

inner layer by inactive motion. Thus the increased u- (and w-) component motion in the rough-to-smooth inner layer is responsible for the reduction in R_{12} below the smooth-wall value.

Figure 5 shows the u- and v-component power spectra (ϕ_{11} and ϕ_{22} and respectively) together with the uv cross-spectrum for the near-wall motion of both boundary layers, scaled using $\overline{uv}$ and y and taking the local mean streamwise velocity as the convection velocity. Integrals of the scaled spectra yield the appropriate Reynolds stress divided by $-\overline{uv}$. The arguments outlined in the previous section imply that these spectra obtained at points in the logarithmic region are similar above those wavenumbers at which the inactive motion becomes effective and below those wavenumbers at which the motion begins to be affected by viscosity,

$$0.3 < \omega y/U = k_1 y < 5.0.$$

The smooth-wall spectra all collapse except the one at $y/\delta = 0.17$, but the rough-to-smooth spectra collapse only at the two smallest values of y/δ. Those ϕ_{12} spectra which collapse are accurately universal down to low wavenumbers (smooth, $k_1 y \simeq 0.070$; rough-to-smooth, $k_1 y \simeq 0.035$): there is a slight increase in density at low k_1 in the rough-to-smooth spectrum – evidence of the strong inactive motion in the inner layer. The low-wave-number part of the ϕ_{11} spectra, and to a lesser extent that of the ϕ_{22} spectra, show gross non-similarities as a result of inactive motion. This part of the ϕ_{11} spectra also reveals the largest difference between the spectra for the two layers.

ϕ_{11} and ϕ_{22} are also both universal at wavenumbers typical of the inertial subrange. The solid line represents the usual subrange relation assuming local equilibrium, namely

$$\frac{\phi_{11}}{-\overline{uv}\,y}(k_1) = \frac{C}{\kappa^{\frac{2}{3}}}(k_1 y)^{-\frac{5}{3}}. \tag{2.3}$$

Here $C = 0.5$: a similar expression applies to ϕ_{22}, with $\phi_{22} = \frac{4}{3}\phi_{11}$. Bradshaw (1967*a*) shows spectra obtained in the outer layer of boundary layers in both zero and adverse pressure gradients scaled using $-\overline{uv}$ and δ. For outer-layer spectra, the collapse at wavenumbers typical of the inertial subrange is not as good as that in the inner layer, suggesting that spectral energy transfer is only approximately universal in the outer layer, that is, it is not quite independent of y and only nearly proportional to $(-\overline{uv})^{\frac{3}{2}}/\delta$.

Both Bradshaw (1967*c*) and Tennekes & Lumley (1972) have examined the conditions necessary for the existence of an inertial subrange. Both show that a $k^{-\frac{5}{3}}$ region is possible while relaxing the condition that the spectral transfer of energy equals the dissipation, ϵ. It is a sufficient condition (and the only one that necessarily follows from the form of the inertial subrange law) that sources and sinks within the subrange are small compared with the total dissipation, rather than requiring that the motion be completely isotropic, that is, with a spectral shear correlation coefficient $R_{12}(k_1) = 0$. Bradshaw suggests that the Reynolds number based on the Taylor microscale, $Re_\lambda > 100$ for a subrange with first-order local isotropy: our measurements show that $Re_\lambda \simeq 160$ for traverse points closest to the wall ($y^* \simeq 250$) in both layers. At the low-wavenumber end of the subrange (say, $k_1 y \simeq 1.8$), $R_{12}(k_1) = 0.34$ and 0.26 in the smooth and rough-to-smooth layers respectively, falling rapidly with increasing k_1. Mestayer (1982) shows that, in an 'expected' inertial subrange deduced by a small overlap in the production and dissipation spectra, the $-\frac{5}{3}$ law is approximately obeyed and $R_{12}(k_1) \simeq 0.1$. *The* $-\frac{5}{3}$ slope is accurately obeyed over a small range of higher wavenumbers in which $R_{12}(k_1) = 0$ and

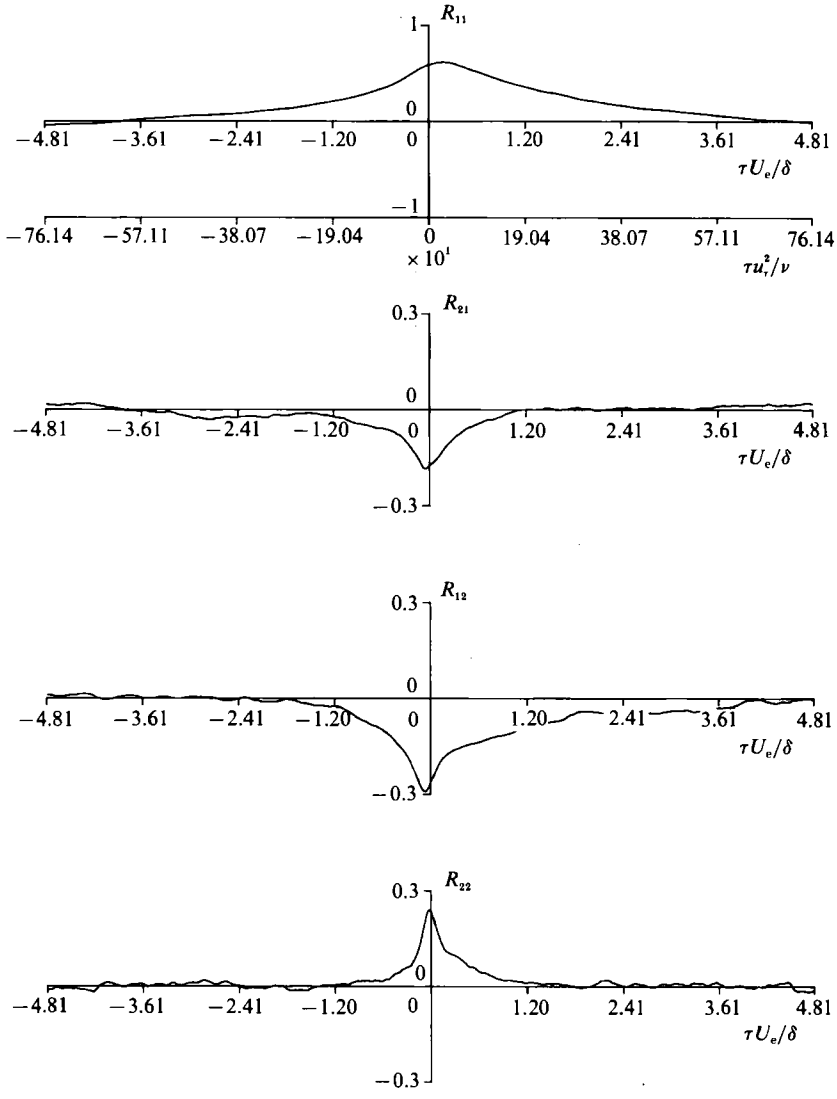

FIGURE 6. Space–time velocity correlation coefficients with vertical separations R_{12}, R_{21}, R_{12}, R_{22}. First subscript refers to 'fixed' probe at $y/\delta = 0.051$. Second subscript refers to 'moving' probe $r_2/\delta = 0.073$.

the production spectrum tails off to zero. Saddoughi *et al.* (1991) have recently shown that, in a boundary layer of 1 m thickness where $Re_\theta \simeq 3 \times 10^5$, ϕ_{11} shows two decades of $-\frac{5}{3}$ with only the second (at higher wavenumber) having $R_{12}(k_1)$ acceptably close to zero. Direct numerical simulation (DNS) has enabled a closer study of inertial energy transfer in isotropic turbulence – necessarily at low Reynolds number – (Domaradzki & Rogallo 1990; Yeung & Brasseur 1991), although there is as yet no unanimity on whether the scales involved or the triadic interactions are local or not. The results of Yeung & Brasseur, however, suggest that non-local triadic interactions cause anisotropy of the dissipative scales of motion which persists at high Reynolds number.

Figure 6 shows smooth-wall space–time correlations, $R_{ii}(r_2;\tau)$, in which the hot wires are separated vertically: the lower wire is at $y/\delta = 0.051$ and the separation,

r_2/δ is 0.073. Similar results were obtained for larger separations up to $r_2/\delta = 0.432$, but at even larger separations, the correlations are too small for a reliable interpretation to be made. Positive time delay, τ, corresponds to downstream displacement of the upper probe relative to the lower one. The correlation subscripts are such that the first refers to the lower probe. Both R_{11} and R_{22} are skewed to positive time delay, an indication of the prevalence of structures inclined at a positive angle to the x-axis; the former actually peaks at $\tau U_e/\delta = 0.25$, a delay equivalent to an inclination of about 16° to the x-axis. R_{11} and (to a lesser extent) R_{22} can be taken as illustrations of the motion of the large-scale structure. R_{21} and R_{12} are also anti-symmetric but give a qualitative indication of ejections and sweeps since they are both negative for all τ. R_{21} is negatively skewed, consistent with an eruption $(+v)$ near the wall correlating with upstream fluid of low momentum further from the wall (quadrant 2 in the (u, v)-plane), or the high momentum fluid at the outer probe causing motion towards the wall at the inner probe further downstream (quadrant 4). R_{12} at positive time delay can be interpreted in a similar fashion, but both correlations agree with the obvious notion that ejections move upstream relative to the mean flow ($u < 0$) and sweeps move downstream ($u > 0$).

Since R_{11} and R_{12} are both skewed to positive time delay and since the tail of R_{12} is particularly long, it seems likely that the main contribution to $R_{12}(+\tau)$ comes from large-scale sweeps and the sense of the probe separation suggests that the front of the large-scale structure is involved. The correlation at negative time delay can therefore be considered as representative of ejections: the sense of the time delay here suggests that the back of the large-scale structure is involved. Both R_{12} and R_{21} suggest a burst-sweep cycle and qualitatively they do not change over nearly the whole boundary layer. This description is consistent with the space–time correlations of Kovasznay *et al.* (1970). These results can be usefully compared with the spatial correlations of Tritton (1967).

3. Ejection and sweep structure

Ejections and sweeps have been detected by applying the VITA + LEVEL algorithm to the instantaneous uv and ω_3 signatures. The cross-wire length is about $70\,\nu/u_\tau$ in both layers: results are presented for $y^* > 250$ so that they can be regarded as independent of wire length. Low-wavenumber measurements of s_{12} and ω_3 were made with a four-wire array for which $\delta x^* = \delta y^* = 306$, $\delta y/\delta_{995} = 0.065$.

The VITA + LEVEL algorithm is applied to a digitized signal, f, and uses two thresholds, VITH and TH, such that an event is detected if:

$$\hat{f} > \mathrm{VITH}\,\overline{f^2}, \quad f > \mathrm{TH}\,(\overline{f^2})^{\frac{1}{2}}, \tag{3.1 a, b}$$

where $\hat{f}$ is the VITA average. When both these criteria are met, the level criterion (3.1 b) is used alone on the signal, either side of the detection point, to determine the beginning and end of an event. The scheme generates an identity trace, $I(t)$ which equals unity when these criteria are satisfied and zero otherwise. The identity ratio, γ is the average of $I(t)$.

The most important aspect of the uv-based scheme is that the thresholds are universal multiples of the local value of $-\overline{uv}$. The effect of changes in threshold (in particular, TH which is the one that effectively determines the length of an event) was investigated by Morrison *et al.* (1989). Obviously, raw conditional statistics are threshold dependent, but they showed that, for example, the scalings of event lengths with y are independent of threshold, within sensible limits. In the present

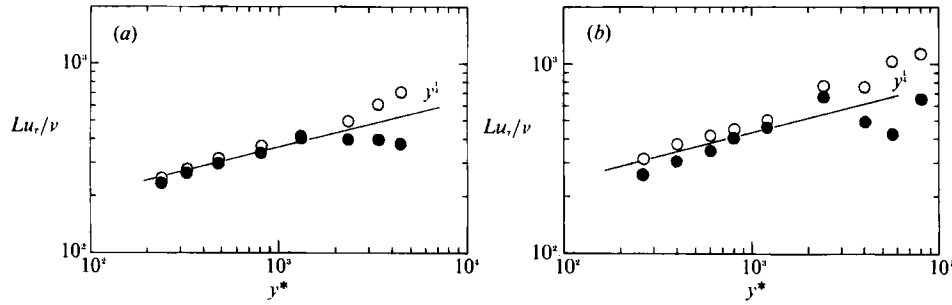

FIGURE 7. Event lengths sampled using uv; (a) smooth; (b) rough-to-smooth. ●, $u > 0$, $v < 0$; ○, $u < 0$, $v > 0$. ——, $L \propto y^{\frac{1}{4}}$.

work, thresholds were largely determined by examination of instantaneous signal and identity traces. Subsequently, Chen & Bradshaw (1990) recommended a value of TH very close to the one used here.

Velocity statistics are presented principally in two ways: for example, $\gamma\widetilde{uv}/(\overline{u^2v^2})^{\frac{1}{2}}$ represents the contribution made by all events to R_{12} whereas $\widetilde{uv}/(\widetilde{u^2}/\widetilde{v^2})^{\frac{1}{2}}$ is the event-averaged correlation coefficient that uses only averages accumulated while the conditioning criteria are satisfied. In all cases, the conventional averages of U and V are used as the baselines from which u and v are measured. In the present work, comparison of these two types of correlation has been particularly illuminating, and has for instance shown that while the contribution by 'eventful' turbulence to the total R_{12} may be quite small, the event-averaged R_{12} may be numerically as large as -0.85.

3.1. *uv-Conditioned statistics*

Here the sampling scheme is supplemented by a quadrant analysis in which only $u > 0$, $v < 0$ (sweep) and $u < 0$, $v > 0$ (ejection) quadrants are retained. The decision is made at the centre of the event i.e. a single point half way between the beginning and end. Superscripts '+' and '−' denote sweep and ejection quantities respectively. Conditionally averaged quantities follow the summation convection:

$$\gamma^+(-\overline{uv}^+)+\gamma^-(-\overline{uv}^-)=\gamma(-\widetilde{\overline{uv}}), \tag{3.2}$$

where

$$\gamma^+ + \gamma^- = \gamma,$$

and γ is typically about 0.15 in this case. Note also that powers of uv and other variables satisfy the general relation:

$$\gamma^+\overline{u_i^n u_j^m}^+ + \gamma^-\overline{u_i^n u_j^m}^- + (1-\gamma)\,\widetilde{\overline{u_i^n u_j^m}} = \overline{u_i^n u_j^m} \tag{3.3}$$

for $n \geqslant 0$, $m \geqslant 0$. '$\approx$' represents a 'turbulent' average whereas '$\simeq$' indicates a non-turbulent average: the tilde for event averages is dropped since these are 'turbulent' anyway. Further details of the quadrant analysis and summation of the averages are given in Morrison, Tsai & Bradshaw (1986). R_{12}^+ represents the sweep contribution

$$\gamma^+(-\overline{uv}^+)/(\overline{u^2}\,\overline{v^2})^{\frac{1}{2}}$$

to the total R_{12} correlation. Event correlation coefficients $[(-\overline{uv}^+/(\overline{u^{2+}}\,\overline{v^{2+}})^{\frac{1}{2}}$ are written as $[-\overline{uv}/(\overline{u^2}\,\overline{v^2})^{\frac{1}{2}}]^+$.

Figure 7 shows event lengths, L, calculated as the product of the first moment of the probability distribution function (p.d.f.) of event durations and the local mean velocity and scaled using ν/u_τ. Over most of the logarithmic layer in the smooth-wall flow, both ejection and sweep lengths vary as $y^{\frac{1}{4}}$, like the variation of the Kolmogorov lengthscale, $\eta \equiv (\nu^3/\epsilon)^{\frac{1}{4}} \simeq y^{\frac{1}{4}}(\nu/u_\tau)^{\frac{3}{4}}$ deduced by assuming local equilibrium. The p.d.f.s

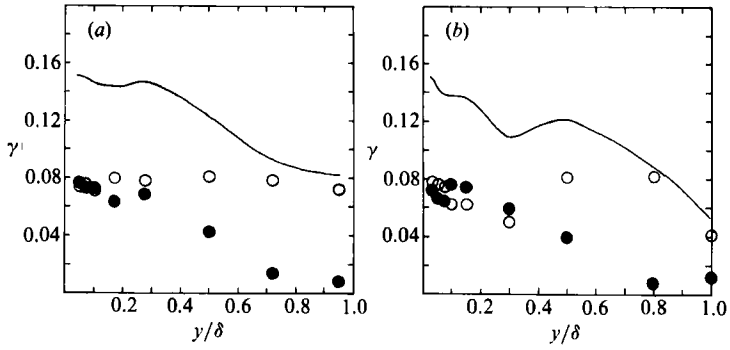

FIGURE 8. uv-event identity ratios: ●, γ^+; ○, γ^-; ——, $\gamma = \gamma^+ + \gamma^-$; (*a*) smooth; (*b*) rough-to-smooth.

are positively skewed with a mean of about 80η, which, for points in the local equilibrium region, roughly coincides with the middle of an expected first-order inertial subrange. In the rough-to-smooth inner layer ($y^* < 400$), event lengths do not follow a $y^{\frac{1}{4}}$ variation. Further from the wall, ejection lengths do appear to do so, but this is fallacious since the same data scaled using $(-\overline{uv})^{\frac{1}{2}}$ or $(-\overline{uv^-})^{\frac{1}{2}}$ do not show a $y^{\frac{1}{4}}$ variation, implying a change of scale and therefore significant advection and turbulent diffusion. In the outer layer, taking $\epsilon \propto u_\tau^3/\delta$ and using u_τ as a non-local velocity scale (independent of y), implies that η is constant and directly proportional to $\delta^{\frac{1}{4}}$. Only sweep lengths are constant in the outer layer and then only approximately so. Ejection lengths appear to increase slightly above the $y^{\frac{1}{4}}$ variation, a change that is consistent with a more rapid reduction in ϵ than its proportionality to $(\overline{uv})^{\frac{3}{2}}/\delta$ would imply. Morrison & Bradshaw (1989) have plotted the same event lengths for the smooth-wall layer as $L(-\overline{uv})^{\frac{1}{2}}/\nu$ *vs.* $y(-\overline{uv})^{\frac{1}{2}}/\nu$, that is using a local velocity scale rather than u_τ. The near-wall $y^{\frac{1}{4}}$ variation persists but for $y/\delta > 0.2$, event lengths fall sharply.

Ejections and sweeps in the log-region of the smooth-wall layer are, on average, near a condition of energy equilibrium. They also dominate the spectral transfer of energy that scales on $(-\overline{uv})^{\frac{3}{2}}$ and y, since the absence of spatial transport implies the absence of sources or sinks in the wavenumber domain. Outer-layer sweeps are, on average, only approximately in equilibrium and here the universal part of spectral energy transfer scales on $(-\overline{uv})^{\frac{3}{2}}$ and δ but is weakly dependent on y. This result alone illustrates the success of a sampling scheme which uses thresholds that are universal multiples of $-\overline{uv}$.

Figure 8 shows the identity ratios (intermittency) of events: ejections occur more frequently than sweeps in the outer layer, and so contribute more to the shear stress there (figure 9). Ejections and sweeps make roughly equal contributions to the shear stress in the inner layers of both boundary layers and occur for roughly the same amount of time. A quadrant analysis of the uv signal without sampling usually indicates that an average accumulated for quadrants two and four only is about $-1.5\ \overline{uv}$ so that our scheme, which samples about 80% of $-\overline{uv}$, has effectively selected about half the negative $\overline{uv}$. But the scheme is intended to maximize $\gamma^+(-\overline{uv^+})^{\frac{3}{2}} + \gamma^-(-\overline{uv^-})^{\frac{3}{2}}$ (i.e. event contributions to spectral energy transfer) rather than $\gamma^+(-\overline{uv^+}) + \gamma^-(-\overline{uv^-})$.

In the region $0.2 < y/\delta < 0.6$ of the rough-to-smooth layer, most of the turbulence was generated on the rough surface. The event contribution to $-\overline{uv}$ is constant in this region but roughly equal to u_τ^2 at B, the measurement station. In a region of

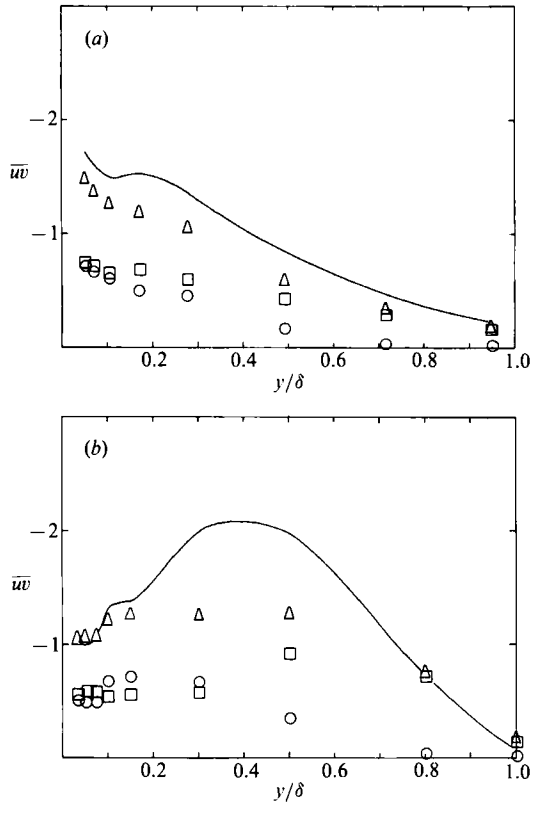

FIGURE 9. uv-event contributions to $\overline{uv}$: (a) smooth; (b) rough-to-smooth. ○, $\gamma^{+}\overline{uv}^{+}$; □, $\gamma^{-}\overline{uv}^{-}$; △, $\gamma^{+}\overline{uv}^{+}+\gamma^{-}\overline{uv}^{-}$; ——, $\overline{uv}$.

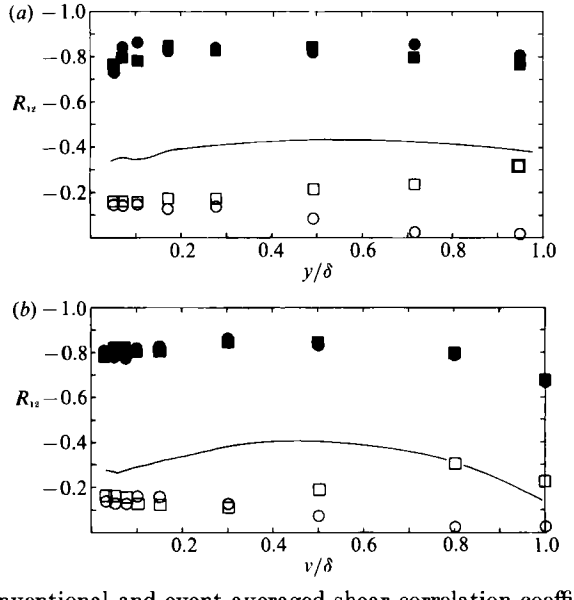

FIGURE 10. Conventional and event-averaged shear correlation coefficients: (a) smooth; (b) rough-to-smooth. ○, R_{12}^{+}; □, R_{12}^{-}; ●, $[-\overline{uv}/(\overline{u^2}\,\overline{v^2})^{\frac{1}{2}}]^{+}$; ■, $[-\overline{uv}/(\overline{u^2}\,\overline{v^2})^{\frac{1}{2}}]^{-}$; ——, R_{12}.

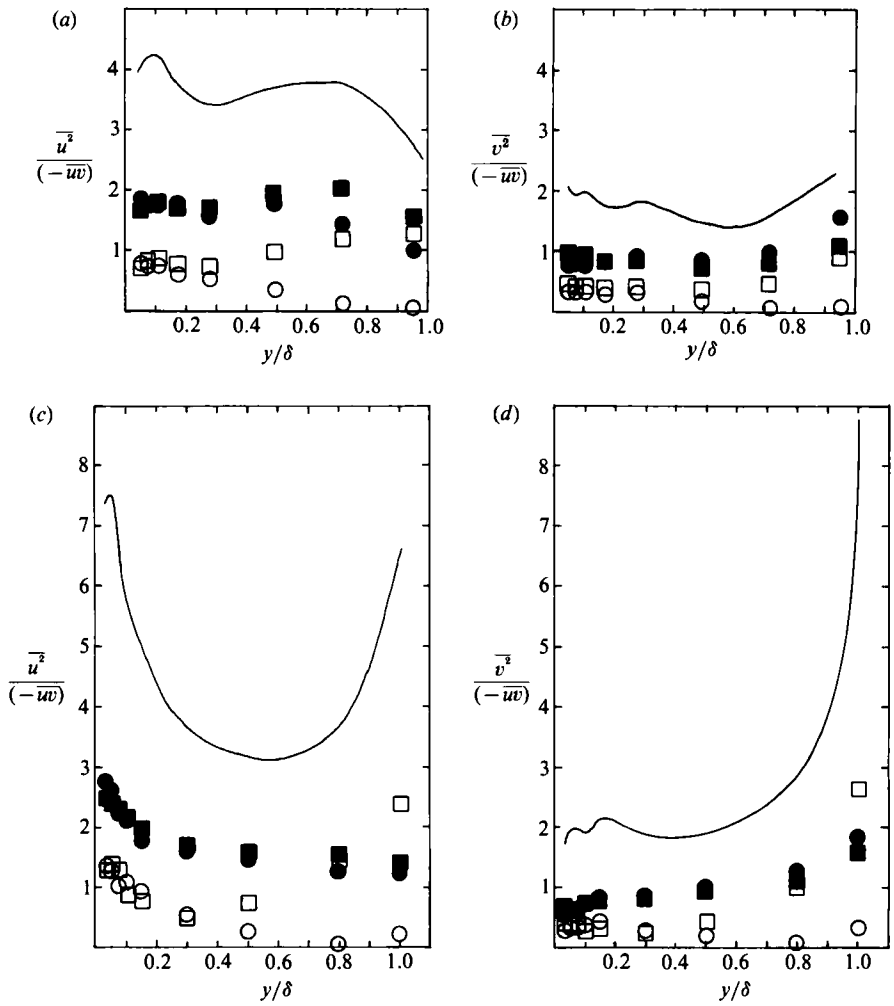

FIGURE 11. Conventional and event-averaged normal stresses (smooth): (*a*) $u^2/(-\overline{uv})$; (*b*) $\overline{v^2}/(-\overline{uv})$. Rough-to-smooth: (*c*) $\overline{u^2}/(\overline{uv})$; (*d*) $\overline{v^2}/(-\overline{uv})$. Symbols as in figure 10 (open symbols, contributions to conventional average; closed symbols, event-averaged quantities; ——, conventional average).

constant R_{12}, the sampling criteria are equivalent to one which selects periods in which $uv/(\overline{u^2}\,\overline{v^2})^{\frac{1}{2}}$ is less than R_{12}, times the threshold. Thus the event contributions to R_{12}, are roughly the same in both layers (figure 10) but those to $-\overline{uv}$ are not, because, in the smooth-wall layer, about 80% of $-\overline{uv}$ has an R_{12} less than the threshold, while in the rough-to-smooth layer this proportion is only about 60%.

Figure 10 also shows the event-averaged values of R_{12} (e.g. $[\overline{uv}/(\overline{u^2}\,\overline{v^2})^{\frac{1}{2}}]^+$) which are consistently between 0.8 and 0.9 for both layers. This implies that both ejections and sweeps are highly coherent and extremely efficient in transporting momentum, which suggests that they are part of a larger inertial structure. This point is explored fully in §5. In some sense, they are a form of 'ultimate' eddy (in the way that the classical derivation of the inertial subrange law by an intermediate limit process might imply) since, although they are affected directly by viscosity, and diffuse slowly because of it, they also, on average, transport momentum (not energy) very effectively when near equilibrium. These properties account for their persistence in

the outer layer at high Reynolds numbers and are illustrated by the behaviour of their triple products in particular.

Figure 11 shows the $\overline{u^2}$ and $\overline{v^2}$ intensities (the w-component was not measured in this work) and figure 12 the corresponding triple products. The use of local $\overline{uv}$ to non-dimensionalize the data is consistent with the spectra of figure 5 and is more general than the use of the wall shear stress used in the derivation of the log law. Since the scaling in figure 7 suggests that events are only weakly dependent on the distance from the wall, a local value of $-\overline{uv}$ seems a sensible scaling. Furthermore, the universal value of $(\overline{pv}/\rho+\frac{1}{2}\overline{q^2v})/(-\overline{uv})^{\frac{3}{2}}$ (assuming the numerator to be a value for the active motion only), indicates that a comparison of the motion of events as a contribution to the whole motion of the layer together with the motion of events considered alone would be worthwhile. ($\overline{q^2}$ is twice the turbulent kinetic energy.) The most striking feature of figure 11 is the constancy of the event-averaged values of $\overline{v^2}/(-\overline{uv})$, generally close to unity. Now, if R_{12} is -1.0 and $\overline{v^2}/(-\overline{uv})$ is constant and equal to p, say, then $\overline{u^2}/(-\overline{uv}) = 1/p$. In the case of event-averaged values of $\overline{v^2}/(-\overline{uv})$, p is near unity whereas this is not so for event-averaged values of $\overline{u^2}/(-\overline{uv})$ which show a similar trend to the corresponding conventional average. Therefore the reason why event-averaged values of R_{12} do not equal -1.0 is primarily the inactive u-component motion included in these events. The contribution to both $\overline{u^2}$ and $\overline{v^2}$ by ejections is greater than that by sweeps over the whole thickness of both boundary layers. The combined contribution by sweeps and ejections is about 40% of $\overline{u^2}/(-\overline{uv})$ and $\overline{v^2}/(-\overline{uv})$, almost half their contribution to the shear stress.

Over the whole thickness of the smooth layer, the conventional averages of the triple products (figure 12) are very nearly equal to the corresponding combined event contributions (i.e. ejections plus sweeps), suggesting that ejections and sweeps dominate inertial transport of energy and shear stress. Since ejections and sweeps, if correctly detected, are by definition the active (but not necessarily universal) motion of the boundary layer, it appears that $\frac{1}{2}\overline{q^2v}$ is mostly active motion. In the rough-to-smooth layer, $y/\delta < 0.1$, there are significant differences between the combined ejection and sweep contributions and their conventional products. In the case of $\overline{u^2v}$ and $\overline{v^3}$, this is evidence of inactive diffusion in the internal layer, to a lesser degree, apparent in the smooth-wall data also. The near-wall ejection and sweep lengths of figure 7 (*b*) show that there is also significant active diffusion and this accounts for a negative value of say, $\partial/\partial y(\overline{v^3}/(-\overline{uv})^{\frac{3}{2}})^+$ in figure 12 (*h*), $y/\delta < 0.1$. This is not apparent in the same data for the smooth layer (figure 12 *d*).

The non-universality of ejections in the outer layer is consistent with the large increase above the inner-layer values in the contribution by ejections to $\overline{u^2v}$ and $\overline{v^3}$. Meanwhile, the contributions by sweeps change by a small but significant amount and this conforms with the view that sweeps represent the near-universal motion of the outer layer. In fact, the small increase in sweep contributions at large y/δ probably explains why the velocity spectra of Bradshaw (1967*a*) do not collapse in the inertial subrange as well as those of figure 5 in the inner layer. Since the outer-layer ejections are far from local equilibrium, it is difficult to make any sensible inferences about their likely effect on any particular wavenumber range of the corresponding spectra. The sense of the outer-layer diffusion by ejections and sweeps is away from the wall and is therefore consistent with Townsend's active diffusion. In the rough-to-smooth internal layer, inactive diffusion of energy by $\overline{q^2v}$ towards the wall is supplemented by the active diffusion of the sweeps caused by a secondary peak in energy or shear stress at mid-layer.

The best assessment of the quality of these data comes from a comparison of event-

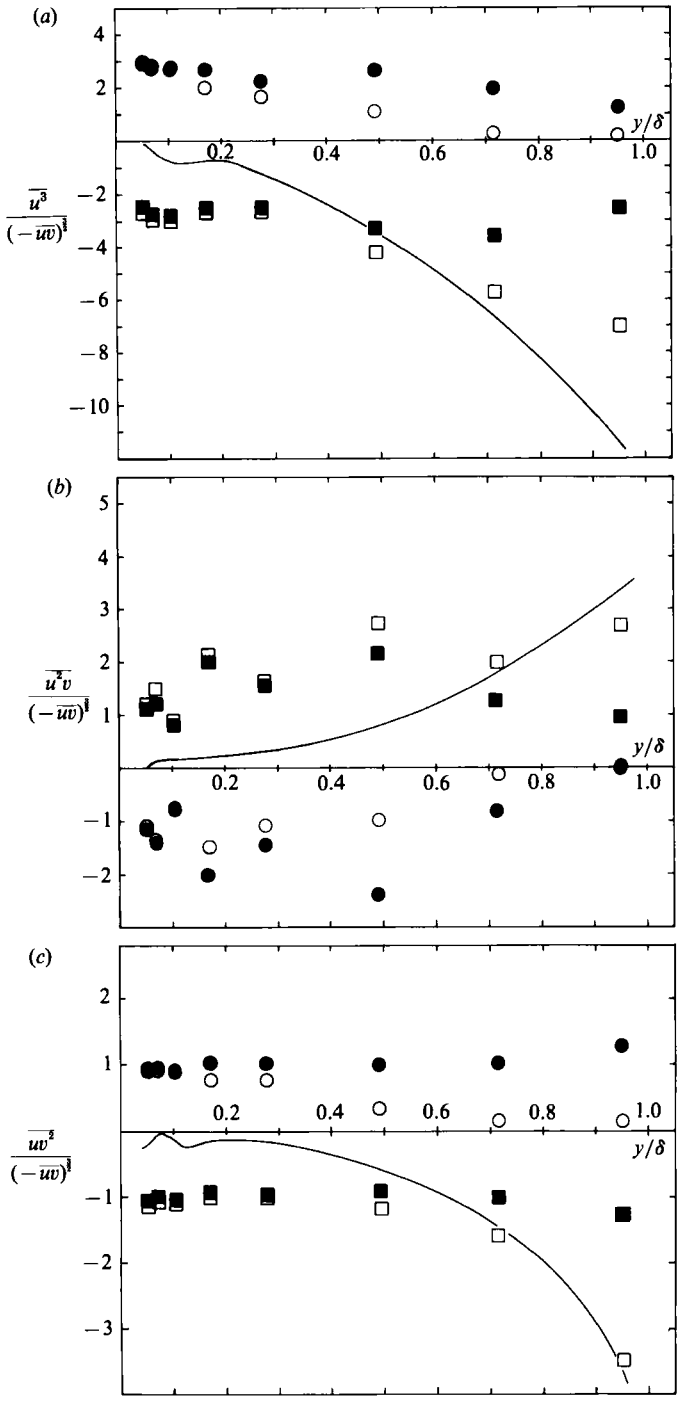

FIGURE 12(*a–c*). For caption see page 93.

averaged statistics (e.g. $[\overline{uv^2}/(-\overline{uv})^{\frac{3}{2}}]^+$) with the same data expressed as a contribution $(\gamma^+\overline{uv^2}^+/(-\overline{uv})^{\frac{3}{2}})$. In the smooth-wall inner layer, these two averages take very nearly the same values: in other words, the velocity scale for sweeps, $(-\overline{uv}^+)^{\frac{1}{2}}$ is the same as that for the whole motion, namely $(-\overline{uv})^{\frac{1}{2}}$, provided due account is

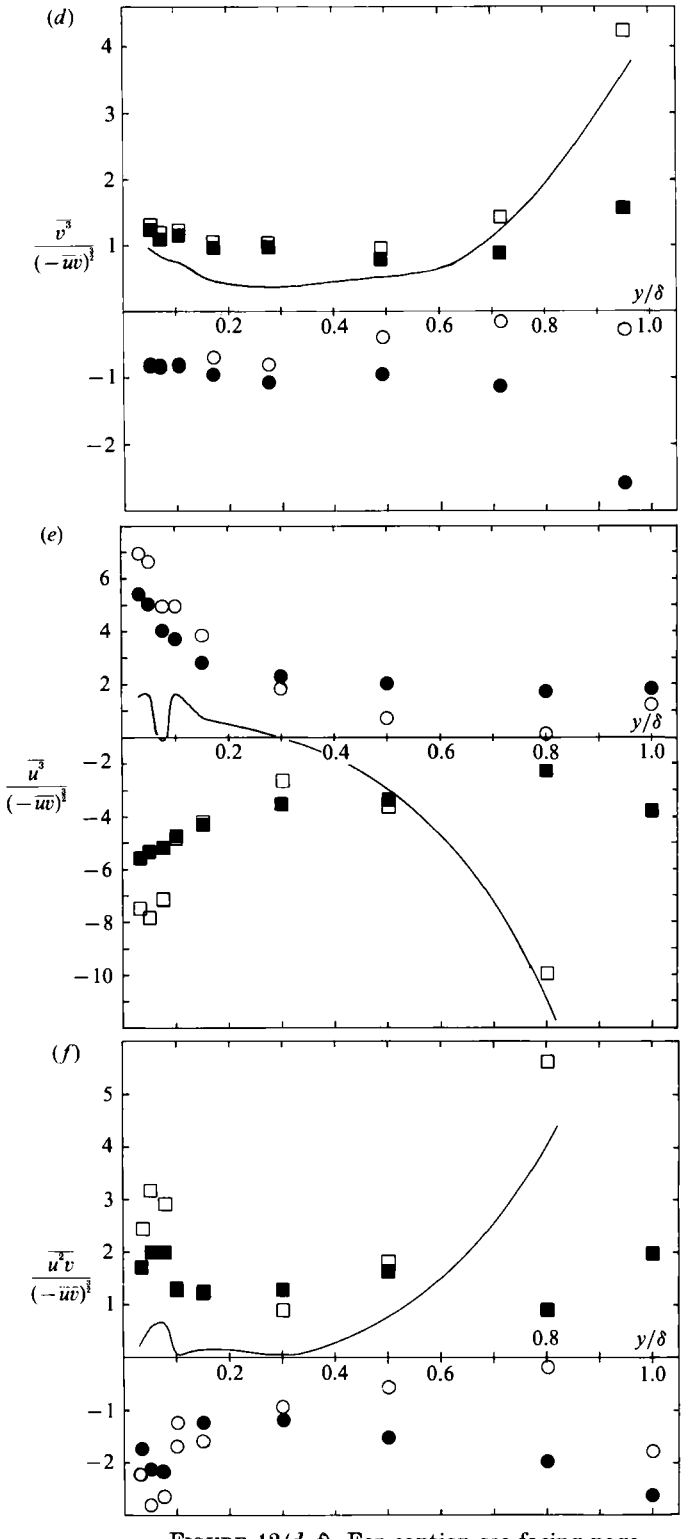

FIGURE 12(*d–f*). For caption see facing page.

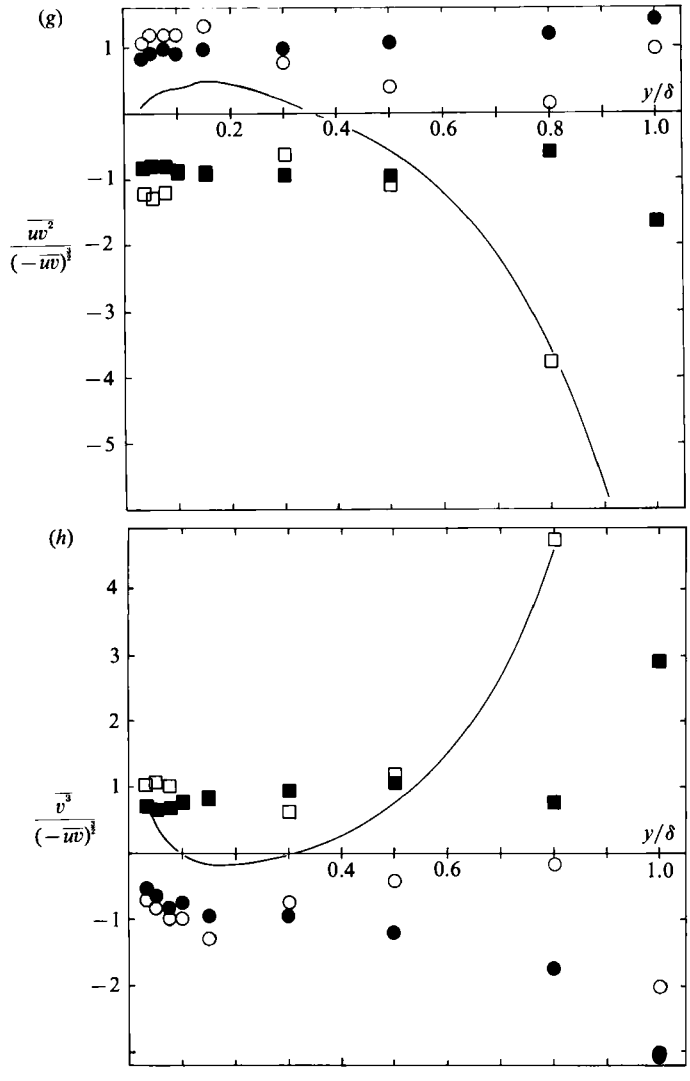

FIGURE 12. Triple products (smooth): (*a*) $\overline{u^3}/(-\overline{uv})^{\frac{3}{2}}$; (*b*) $\overline{u^2v}/(-\overline{uv})^{\frac{3}{2}}$; (*c*) $\overline{uv^2}/(-\overline{uv})^{\frac{3}{2}}$; (*d*) $\overline{v^3}/(-\overline{uv})^{\frac{3}{2}}$. Rough-to-smooth: (*e*)–(*h*) in same sequence. Symbols as in figure 11.

taken of the proportion of time over which each is averaged. The implication is that the present results agree with Townsend's hypothesis that the active diffusion takes a universal value only in a local equilibrium layer, so that in the rough-to-smooth inner layer, the event contributions and the event averages diverge as a consequence of there being no single, universal velocity scale. A single velocity scale that applies to ejections and sweeps alike, as in the smooth-wall inner layer, implies that:

$$\gamma^+(-\overline{uv}^+)^{\frac{3}{2}} \simeq (-\overline{uv})^{\frac{3}{2}} \simeq \gamma^-(-\overline{uv}^-)^{\frac{3}{2}}, \tag{3.4}$$

so that therefore:

$$\gamma^+(-\overline{uv}^+)^{\frac{3}{2}} + \gamma^-(-\overline{uv})^{\frac{3}{2}} \simeq 2(-\overline{uv})^{\frac{3}{2}}. \tag{3.5}$$

This obviously suggests that:

$$\gamma^+\frac{(-\overline{uv}^+)^{\frac{3}{2}}}{y} + \gamma^-\frac{(-\overline{uv}^-)^{\frac{3}{2}}}{y} \simeq \frac{(-\overline{uv})^{\frac{3}{2}}}{Cy}, \tag{3.6}$$

where $C = 0.5$. Chen & Bradshaw (1990) recommend a slightly higher threshold than

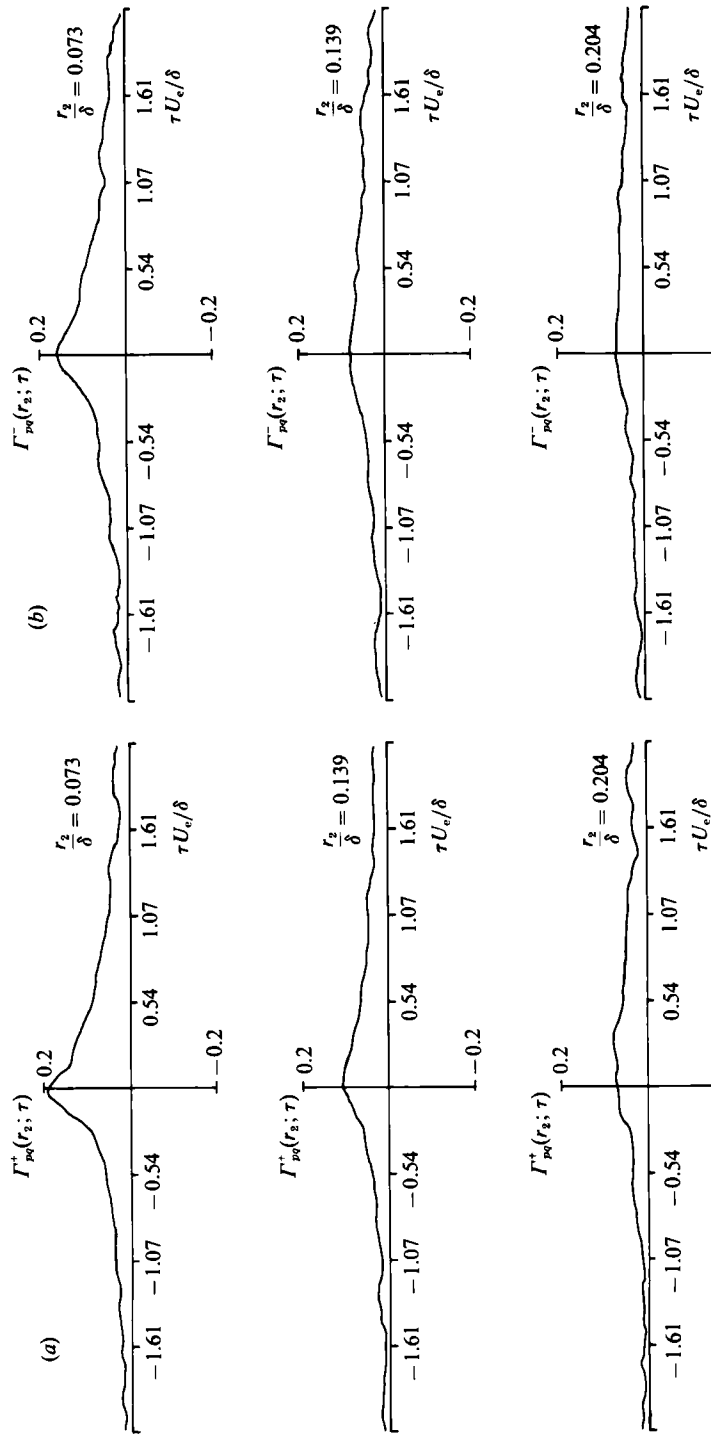

FIGURE 13. Identity-trace correlation coefficients (smooth): (*a*) $\Gamma^+_{pq}(r_2;\tau)$; (*b*) $\Gamma^-_{pq}(r_2;\tau)$. Fixed probe '*p*' at $y/\delta = 0.051$.

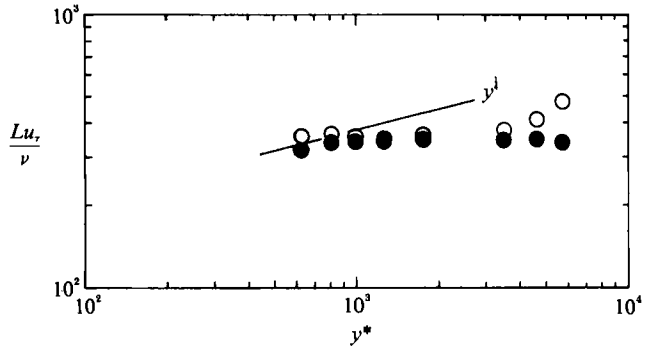

FIGURE 14. ω_3-sampled event lengths (smooth): ●, $\omega_3 > 0$; ○, $\omega_3 < 0$. ——, $L \propto y^{\frac{1}{2}}$.

the one used in this work in order to optimize agreement with visually identified ejections and sweeps from channel-simulation data. Clearly, a slightly higher threshold would imply that $C \simeq \kappa$. The right-hand side of (3.6) implies not only that the universal part of spectral transfer is proportional to $(-\overline{uv})^{\frac{3}{2}}/y$, but also that it is equal to $\gamma(-\overline{uv})^{\frac{3}{2}}/y$.

The $y^{\frac{1}{2}}$ dependence of event lengths suggests that a two-point vertical correlation of event statistics will not show any appreciable correlation. As a test of the feasibility of conducting two-point sampling, we generated space–time correlations of the zero-one identity traces, $I(t)$ produced from VITA+LEVEL detections of simultaneous uv signals from each of a vertical array of four cross-wires. The correlation coefficient is defined as:

$$\Gamma^+_{pq}(r_2;\tau) = \frac{\overline{(I^+_p-\gamma^+_p)\,(I^+_q-\gamma^+_q)}}{(I^+_p-\gamma^+_p)'\,(I^+_q-\gamma^+_q)'} \tag{3.7}$$

for sweeps, where the first subscript refers to the fixed wire closer to the wall. The prime denotes an r.m.s. value and replacement of the ' + ' sign with a ' − ' sign would denote ejections. The use of $(I-\gamma)$ ensures that the two functions (suffices p and q) each have a zero mean value as suggested by Kovasznay *et al.* (1970). The correlations were generated by a standard fast Fourier transform routine. The sense of the time delay is the same as that of figure 6, which provides a useful comparison. Figures 13 (*a*) and 13 (*b*) each show three correlations from the smooth-wall layer. The position of the fixed probe and the three positions of the moving probe correspond roughly to the four y locations at which the spectra in figure 5 (*a–c*) were obtained. These correlations are appreciably smaller than those of figure 6 and, with the exception of the values at the smallest separation, do not show any asymmetry in time that occurs in the R_{12} and R_{21} correlations. Γ^+_{pq} does show some consistency with R_{12} in figure 6, but Γ^-_{pq} is confusingly the same as the sweep correlation.

It is evident that our events represent only part of the integral scales of motion. The smallness of the correlation also implies that individual events are not very well correlated with each other. This is probably partly due at least to the fact that no attempt has been made to change the probe positions relative to each other to account for likely burst trajectories.

3.2. ω_3-*Conditioned statistics*

Figure 14 shows event lengths generated by applying the VITA+LEVEL algorithm to the ω_3 signature in the smooth-wall layer. Events are sorted according to the sign of ω_3 at the event centre with the additional requirement that $uv < 0$ at that time also.

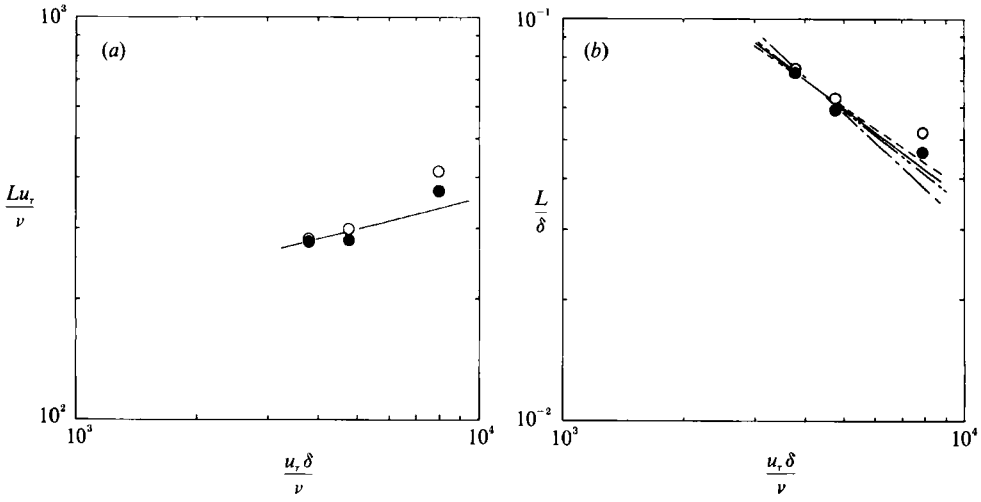

FIGURE 15. uv-event lengths *vs.* $u_\tau\delta/\nu$: (*a*) wall variables; ——, $Lu_\tau/\nu \propto (u_\tau\delta/\nu)^{\frac{1}{4}}$; (*b*) outer variables; ——, $L/\delta \propto (u_\tau\delta/\nu)^{-\frac{3}{4}}$; – – – –, $(C_x/\delta) = 168.23\,Re_\theta^{-0.85}$; – – – – – –, $C_y/\delta = 34.82\,Re_\theta^{-0.728}$. C_x and C_y defined by Falco (1974). – – – –, $L_x/\delta = 17.65\,Re_\theta^{-0.6348}$ (Murlis *et al.* 1982). Other authors' data assumes $u_\tau\delta/\nu \propto Re_\theta^{0.92}$.

This is justified on the argument that we are concerned only with the negative-uv, active part of the motion. In fact, removal of the uv criterion did not reduce the contribution by events to $\overline{uv}$ although $[\overline{uv}/(\overline{u^2}\,\overline{v^2})^{\frac{1}{2}}]^+$ and $[\overline{uv}/(\overline{u^2}\,\overline{v^2})^{\frac{1}{2}}]^-$ were approximately halved by its exclusion. The effect of the additional uv criterion is therefore to improve the coherence of the educed structures. Event-averaged values of R_{12} are generally 0.6 to 0.7 and events make up approximately 40% of $-\overline{uv}$. Event-averaged triple products do not appear to be as useful as those of figure 12, but it is not possible to say whether this is a genuine conclusion or a feature of only low-wavenumber sampling of ω_3.

The $y^{\frac{1}{4}}$ variation is again apparent, but only for $y^* < 900$ ($y/\delta < 0.19$), and at larger y^*, ($\omega_3 < 0$)-event lengths follow those of ejections while ($\omega_3 > 0$)-event lengths follow those of sweeps in figure 7(*a*). This suggests that negative ω_3 dominates in ejections while positive ω_3 dominates in sweeps. This result is consistent with our physical description of ejections and sweeps in the next section. The tendency of event lengths to a constant value at a lower y^* than in the case of figure 7(*a*) is consistent with using a hot-wire array which is intended to resolve only the outer-layer large-eddy processes controlled by a constant lengthscale.

3.3. *Physical description of ejections and sweeps*

Assuming that, in the outer layer, $\epsilon \propto u_\tau^3$, it follows that $\eta u_\tau/\nu \propto (u_\tau\delta/\nu)^{\frac{1}{4}}$, and that $\eta/\delta \propto (u_\tau\delta/\nu)^{-\frac{3}{4}}$. The same results are derived for the log region if $\epsilon \propto u_\tau^3/y$ and $y/\delta =$ constant. Figure 15 shows our uv-sampled event lengths taken at a constant value of $y/\delta = 0.084$ in both layers, as well as in the smooth layer at a slightly lower Reynolds number. Both ejections and sweeps suggest a $(u_\tau\delta/\nu)^{\frac{1}{4}}$ dependence in figure 15(*a*) and a $(u_\tau\delta/\nu)^{-\frac{3}{4}}$ dependence in figure 15(*b*) because event lengths are proportional to η. The rough-to-smooth data deviate from these scalings because log region events are not in equilibrium. Thus the use of a single length and velocity scale used in our estimate of ϵ is not valid.

Also plotted in figure 15(*b*) is the variation of the 'most-probable' outer-layer turbulent-zone length estimated by Murlis *et al.* (1982) using a temperature-based

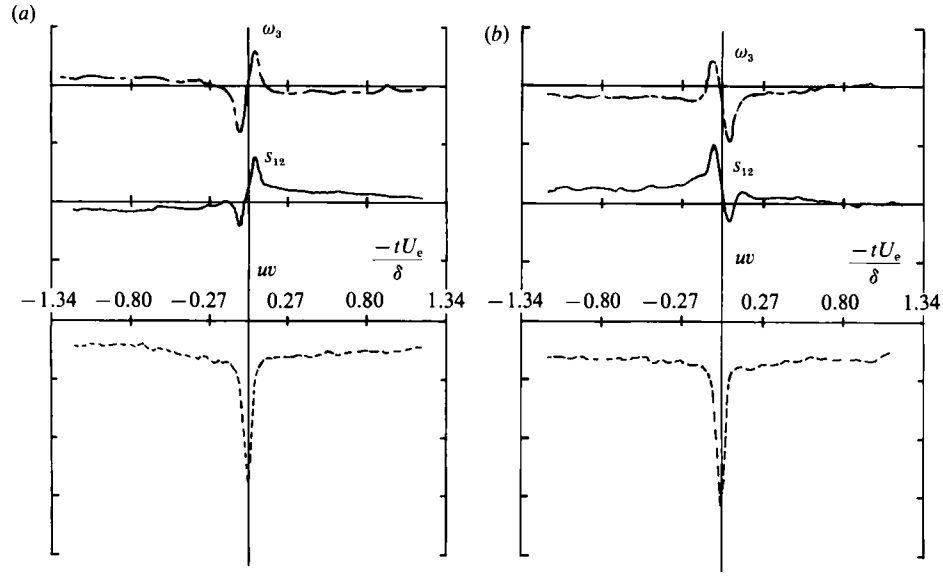

FIGURE 16. uv-event ensemble-averaged time-histories (smooth): (*a*) sweeps; (*b*) ejections. – – – –, uv; – – – – –, ω_3; ——, s_{12}. Vertical scale: one increment = $\frac{3}{4}$ r.m.s. of signal or $(\overline{u^2}\,\overline{v^2})^{\frac{1}{2}}$ in the case of uv.

scheme. Most interestingly, we have also plotted Falco's (1974) estimates for the streamwise and vertical dimensions of the typical eddy, C_x and C_y respectively. We originally assumed that, for all three data sets, $u_\tau \delta/\nu \propto (U_e \theta/\nu)^{\frac{3}{4}}$, which Coles' (1962) data show to be approximately true. However, we are indebted to one of the referees for pointing out that, for $Re_\theta > 3000$, the assumptions that $u_\tau \delta/\nu \propto Re_\theta^{0.92}$ is a better fit to both Coles' and newer data. With this assumption, the agreement in figure 15(*b*) between $L/\delta \propto (u_\tau \delta/\nu)^{-\frac{3}{4}}$ and the other authors' data is improved, the agreement being best for Falco's values of C_y.

Figure 16 shows ensemble-average time-histories for ejections and sweeps obtained by applying the VITA + LEVEL scheme to the uv signal obtained from a four-wire array which can also give estimates of ω_3 and s_{12}. (The array used is the same as that for the ω_3-sampled data of the previous section.) The traces of all the gradient quantities do not change qualitatively with y/δ, even for data outside the log region. Figure 17 is a sketch of a typical eddy taken from Falco (1979, figure 10) with qualitative ω_3, s_{12} and uv signatures for the top lobe superimposed. The thick solid line is the outline of the upper lobe, the thick dashed line is the outline of the lower lobe which Falco usually observed with the upper lobe. The appearance of both lobes is consistent with a cut through a vortex ring in the (x, y)-plane. The large peaks in ω_3 and s_{12} in figure 16(*b*) coincide with those for the top lobe of the typical eddy in figure 17. Our signals also show secondary peaks ($+\omega_3$ and $-s_{12}$ just upstream and downstream of $x = 0$ respectively) that correspond to the expected signals for the lower lobe.

The distinguishing feature of sweeps (figure 16*a*) appears to be that the vorticity is increasing (with x) through the large negative peak in uv. This would correspond to the reflection of the typical eddy about the line joining the two centres of vorticity, and sweeps look as if they are inverted mushrooms moving down towards the wall. The signs of vorticity are what one might expect as a result of high-speed fluid moving toward the wall and being flattened by fluid of lower streamwise momentum or the wall itself, as in the early stages of pocket evolution. Based on these ensemble-

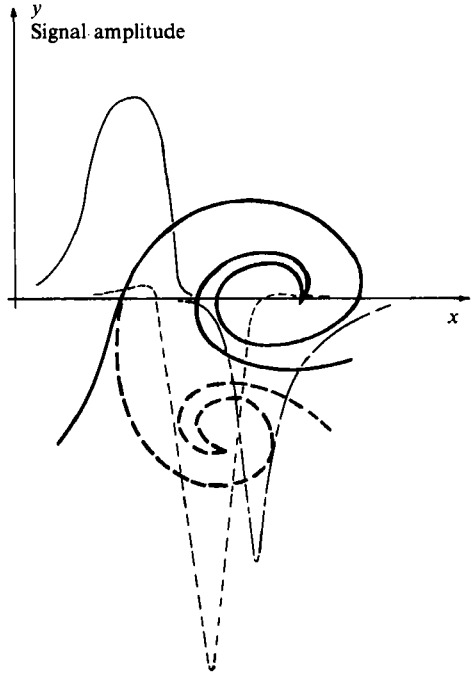

FIGURE 17. Sketch of typical eddy (bold lines) with representative signals (after Falco). Signals as in figure 16.

averaged time-histories alone, both ejections and sweeps appear to have a vortex ring-like structure as suggested by Falco (1983, 1984). Because the signals representative of the lower lobe in an ejection and the upper lobe in a sweep are smaller than those on the other side of the peak in uv, it is possible that the hypothesized vortex ring is not always complete, that is, the hairpin vortex does not always pinch off completely. Furthermore, the large negative peak in ω_3 in the top lobe of an ejection becomes the large negative peak in ω_3 in the lower lobe of a sweep: this implies at 180° clockwise rotation (as in figure 17) for an ejection to become a sweep, that is, as the eddy is toppled by mean vorticity. Falco *et al.* (1989) have recently measured joint p.d.f.s of spanwise vorticity from probes separated vertically but both at $y^* < 30$. These results indicate that the most probable combination is one of $-\omega_3$ at the lower probe and $+\omega_3$ at the upper probe, as the results for a sweep would suggest. Introduction of positive vorticity at the wall initiates a pocket. Irrespective of whether pinching occurs or not, both these results and those of the previous section indicate that negative ω_3 dominates in ejections while, in the case of sweeps, positive ω_3 is at least larger than in an ejection at the same y^*. Apart from the striking similarity of our signals with those of Falco, the peaks in uv are also consistent with the simulations of Kim (1985), who found large uv at the tips of hairpins, and those of Moin *et al.* (1986). In this case, they noted that peaks in uv occurred just downstream of their vortex ring.

4. Ejections, sweeps and energy equilibrium

Figure 18 shows estimates of the total production together with the sum of the spectral transfer effected by uv-events as given by the left-hand side of (3.6). In the smooth-wall layer, only for $y/\delta > 0.1$ do uv-event contributions underestimate the

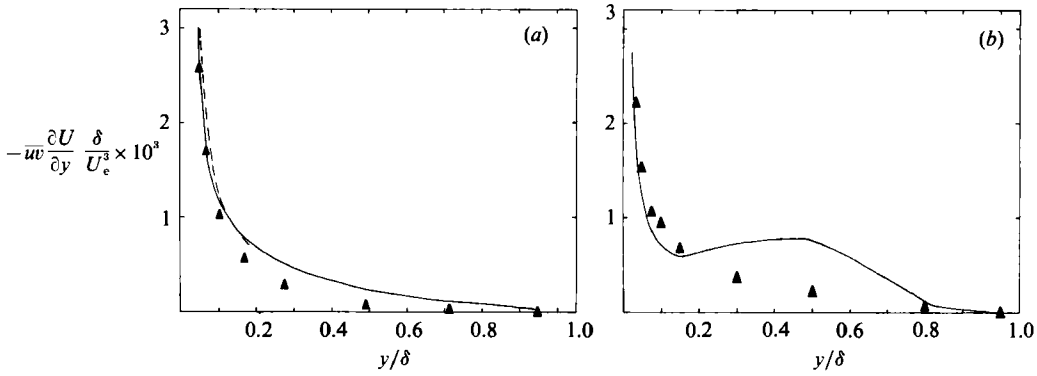

FIGURE 18. Energy production rates: (*a*) smooth; (*b*) rough-to-smooth. ——, $-\overline{uv}(\partial U/\partial y)/(\delta/U_e^3)$; – – – –, $[(-\overline{uv})^{\frac{3}{2}}/y](\delta/U_e^3)$; ▲, $[\gamma^+(-\overline{uv}^+)^{\frac{3}{2}}/y+\gamma^-(-\overline{uv}^-)^{\frac{3}{2}}/y](\delta/U_e^3)$.

y/δ	C (equation (3.6))
0.051	0.48
0.069	0.49
0.103	0.48
0.170	0.55

TABLE 1. Estimates of the von Kármán constant in smooth-wall boundary layer

total production. The use of (3.6) in the rough-to-smooth inner layer gives an overestimate of the production because of sweep diffusion towards the wall: the sweep velocity scale, $(-\overline{uv}^+)^{\frac{1}{2}}$, is still affected by the peak in $-\overline{uv}$ at mid-layer, a relic of the rough-wall turbulence. The secondary peak at mid-layer in figure 18(*b*) is also caused by the larger rough-wall skin friction: both $\overline{uv}$ and $\partial U/\partial y$ are increased here as a consequence.

The validity of (3.6) can be examined by rearranging it to give:

$$L_\tau = \left[\frac{(-\overline{uv})^{\frac{3}{2}}}{\gamma^+(-\overline{uv}^+)^{\frac{3}{2}}+\gamma^-(-\overline{uv}^-)^{\frac{3}{2}}}\right]y, \tag{4.1}$$

where the dissipation length parameter L_τ is defined as $(-\overline{uv})^{\frac{3}{2}}/\epsilon$ and the left-hand side of (3.6) is used as an estimate for ϵ. In the logarithmic region, the bracketed term in (4.1) (C in (3.6)) should equal the usual value of the von Kármán constant; these values are given in table 1. The local equilibrium approximation ignores inner-layer diffusion, of course, and the advection is even smaller. Therefore the numerator, and possibly the denominator in (4.1), contain the effects of spatial transport which acts as a source or a sink at each wavenumber. However, most of the diffusion is universal so that κ can be expected to be invariant from one local-equilibrium flow to another. Equation (4.1) also raises the question of the Reynolds-number dependence of κ: this will be addressed in §5.

Another definition of a lengthscale for energy transfer is the eddy dissipation lengthscale, $L_\epsilon = (\overline{q^2})^{\frac{3}{2}}/\epsilon = a_1^{-\frac{3}{2}}L_\tau$ where $a_1 = -\overline{uv}/\overline{q^2}$. By analogy with L_ϵ, we define

$$L_\epsilon^+ = \left[\frac{1.5(\overline{u^{2+}}+\overline{v^{2+}})}{-\overline{uv}^+}\right]^{\frac{3}{2}}y \tag{4.2}$$

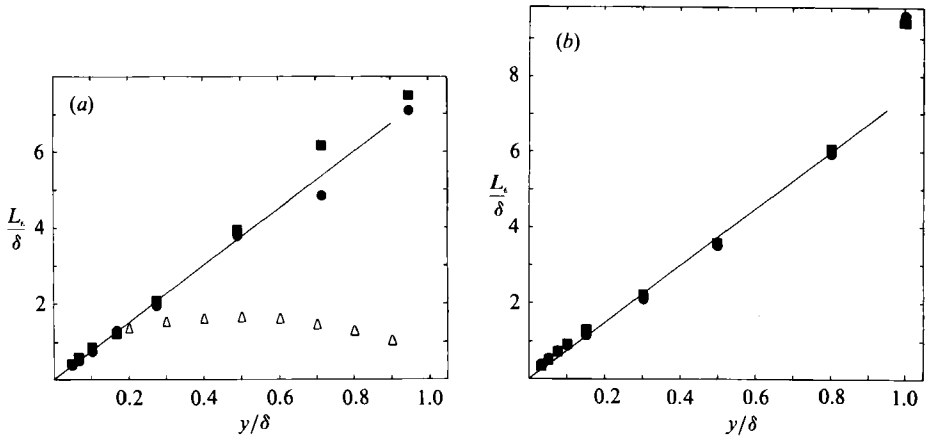

FIGURE 19. Eddy dissipation lengthscales: (*a*) smooth; (*b*) rough-to-smooth. ●, sweeps; ■, ejections; △, conventional: $L_\epsilon = 0.095 a_1^{-\frac{3}{2}} \gamma^{\frac{1}{2}} \delta$. ——, best fit line to L_ϵ^+ and L_ϵ^- ($y/\delta < 0.2$) for which $a_1 = 0.144$.

as a sweep lengthscale, where the numerator is an approximation to $\overline{q^{2+}}$. L_ϵ^- is the equivalent lengthscale for ejections. The purpose of using L_ϵ^+ and L_ϵ^- is that they are defined by event statistics alone, and can be usefully compared with L_ϵ. This is shown in figure 19. For the smooth layer, L_ϵ is derived from the distribution of L_τ given by Bradshaw, Ferriss & Atwell (1967) using the value of $a_1 = 0.15$ which they also used. The solid line represents the best fit to L_ϵ^+ and L_ϵ^- for $y/\delta < 0.2$ and for which $a_1 = 0.144$ when $\kappa = 0.41$. This can be regarded as a value of a_1 for the active motion only. L_ϵ^+ and L_ϵ^- closely follow the local-equilibrium approximation to L_ϵ out to $y/\delta \simeq 0.3$, and thereafter, L_ϵ^+ and l_ϵ^- begin to diverge. L_ϵ^+ and L_ϵ^- are qualitatively similar in the rough-to-smooth layer although the agreement with the local-equilibrium definition of L_ϵ for approximately $y/\delta < 0.2$ is not good, especially in the case of L_ϵ^+. These results confirm what has already been gleaned from the event lengths of figure 7. In figure 19(*b*), the variation of L_ϵ^+ and L_ϵ^- is qualitatively similar to that of the mixing length measurements of Antonia & Luxton (1972), and lie significantly above the local-equilibrium definition of L_ϵ.

An alternative interpretation of κ can be obtained by assuming that $L_\epsilon = L_\epsilon^+ = L_\epsilon^-$ as indicated in the local-equilibrium region of the smooth-wall layer. It follows that:

$$\kappa = (a_1/a_1^+)^{\frac{3}{2}} = (a_1/a_1^-)^{\frac{3}{2}}, \tag{4.3}$$

where the superscripts denote ejection and sweep values. In this case, $1/\kappa$ can be described as the ratio of the efficiency with which ejections or sweeps (or both) transport momentum (not energy) relative to the active flow as a whole:

$$a_1^+ \simeq a_1^- \simeq 0.26 \quad \text{for} \quad y/\delta < 0.2$$

in the smooth-wall layer.

The use of $a_1 = 0.144$ for all values of y in the log region implies that L_ϵ refers to the active motion only: measured values of a_1 drop sharply for $y/\delta < 0.1$ because of inactive motion. Crudely speaking, equations (4.3) are the equivalent definition of κ in physical space to that used in (3.6) for wavenumber space. Substitution of (4.3) into (3.6) gives

$$\gamma^+(\overline{q^{2+}})^{\frac{3}{2}} + \gamma^-(\overline{q^{2-}})^{\frac{3}{2}} = (\overline{q^2})^{\frac{3}{2}}, \tag{4.4}$$

where the right-hand side refers to the active motion only, as a_1 does in (4.3). The common feature to the two definitions of κ is that they both express a quality of ejections and sweeps relative to the active flow as a whole.

Outer-layer results so far presented show that sweeps are the near-universal motion of the outer layer, scale on $(-\overline{uv})^{\frac{1}{2}}$ and δ, and effect only a small degree of spatial energy transport. Our results indicate that

$$\gamma^+(-\overline{uv})\frac{\partial U}{\partial y} \simeq \gamma^+\frac{(-\overline{uv}^+)^{\frac{3}{2}}}{\delta} = \frac{(-\overline{uv}^+)^{\frac{3}{2}}}{L_\tau^+} \tag{4.5}$$

in the outer layer of the smooth-wall layer where $L_\epsilon^+ = \delta/\gamma^+$. In other words, if the outer-layer flow consisted entirely of sweeps (i.e. $\gamma^+ \to 1$), then the right-hand side would give an estimate of the total production with less than 10% error except at thc largest y/δ where the error is 39% and sampling uncertainties high. At the largest y/δ, sweeps occur for less than 1% of the time anyway. Equation (4.5) suggests that sweeps (and not ejections) effect the near-universal component of spectral energy transfer in the outer layer. Not only is the energy transfer proportional to $(-\overline{uv})^{\frac{3}{2}}/\delta$, but it is actually equal to $(-\overline{uv}^+)^{\frac{3}{2}}/\delta$, when averaged only for the time during which sweeps are present, and $\gamma^+(-\overline{uv}^+)^{\frac{3}{2}}/\delta$, when averaged for the whole time. Thus, (4.5) is the outer-layer equivalent of (3.6) for the log region. However, in the outer layer, there are no simple approximations that can be made about the energy balance: thus L_τ^+ is a function of γ^+ which, unfortunately, is not universal for a given threshold because ϵ is not universal. Only if sweeps occupy the whole of the outer-layer motion does the energy balance reduce to the local-equilibrium approximation and $L_\tau^+ = \delta$ and $L_\epsilon^+ = (a_1^+)^{-\frac{3}{2}}/\delta$. The lengthscale of ejections in the outer layer is increasing rapidly (recall figure 7) and this suggests that their contribution to the spectral flux is much diminished by advection or diffusion which act as a net sink at wavenumbers in and above the near-universal range. Equation (4.5) does not include a term for ejection energy transfer because of this. In fact, figure 19(*a*) shows that a_1^+ is approximately constant in the outer layer also (certainly more constant than a_1^-) and, assuming that the spectral transfer of energy effected by ejections is small, then $\epsilon \propto (-\overline{uv}^+)^{\frac{3}{2}}/\delta$. Thus L_ϵ^+ is constant in the outer layer.

5. Discussion

Figure 20 shows correlation lengthscales calculated from $R_{\tau uv}^+$ and $R_{\tau uv}^-$ (i.e. event contributions to the conventional correlation non-dimensionalized by conventional r.m.s. quantities) where τ is the fluctuating wall shear stress as measured by a hot wire mounted in the sublayer. See Morrison & Bradshaw (1989) for details. Thus

$$L_{\tau uv}^+ = \frac{U}{\gamma^+}\int_{-\infty}^{\infty} R_{\tau uv}^+(r_2;\tau)\,\mathrm{d}\tau, \tag{5.1}$$

and the arrows denote estimated errors due to non-zero correlation at maximum time delay. For $y < 0.2\delta$, $L_{\tau uv}^-$ is proportional to y while $L_{\tau uv}^+$ is not. The straight-line fit through the data is not imposed at the origin since inactive 'contamination' of sampled events implies that $L_{\tau uv}^-$ does not tend to zero as $r_2 \to 0$.

These data and those of figure 19 illustrate the major difference between ejections and sweeps, or more accurately, the inertial structures associated with them. The former conform to Townsend's (1976) description of attached eddies, namely: (*a*) that the average eddy size is directly proportional to the distance from the wall, and

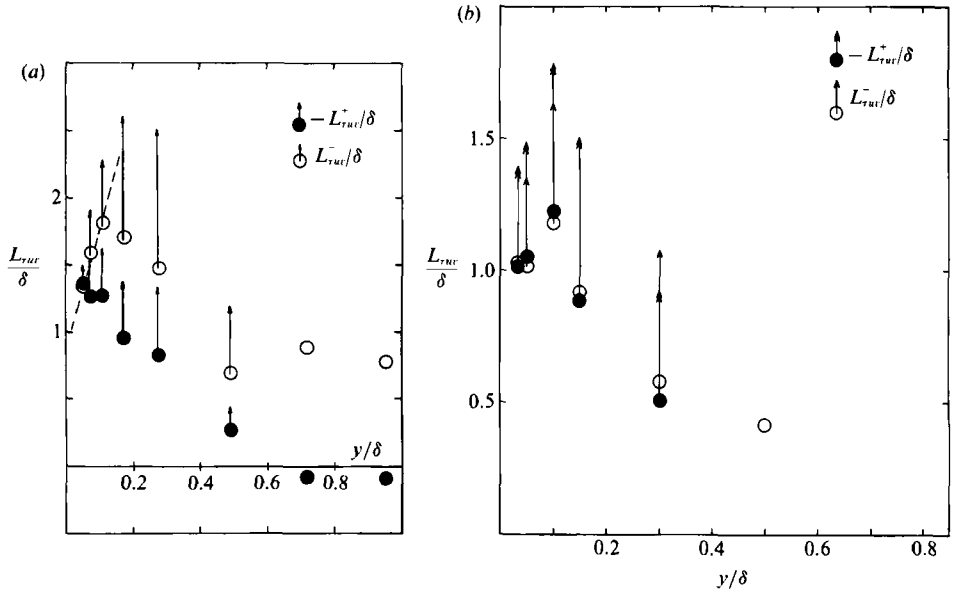

FIGURE 20. Correlation lengthscales, L_{ruv} (*a*) smooth, (*b*) rough-to-smooth: ●, sweeps; ○, ejections.

(*b*), that most of the production and dissipation of energy is concentrated at the 'centre' of the eddy. Moreover, ejections provide most of the difference between the production and dissipation of energy in the outer layer, this being diffused from the inner layer. Ejections therefore control the interaction (in terms of energy, at least) between the inner and outer layers. Comparison between the conditional statistics of the present work and the flow-visualization results (at low Reynolds numbers) of other workers is inevitably tenuous. However, it seems appropriate that, at this stage, the inertial structures associated with ejections be called bursts because they appear to have the dominant characteristics identified by Kline *et al.* (1967) and Kim *et al.* (1971).

On the other hand, although sweeps are large-eddy 'centres' where the inertial transfer of energy is concentrated and which primarily control the distribution of shear stress along with ejections, the associated large eddy produces large, low-wavenumber fluctuations in the u- and w-component motion near the wall which fits Townsend's description as being inactive. See Morrison and Bradshaw (1989) for further results. The correlation lengthscales for the rough-to-smooth layer are less conclusive, partly because of the shorter non-dimensional time delay in the correlations but also because of the lack of data close to the wall, i.e. $y/\delta < 0.05$. However, these data do show that it is unlikely that L^{-}_{ruv} is proportional to y and in general, the variation of L^{-}_{ruv} with y is not noticeably different from that of L^{+}_{ruv}. This result, and those for L^{+}_{e} and L^{-}_{e} in the rough-to-smooth layer (figure 19*b*), illustrate the insensitivity of the mean motion to changes of scale: in the log region of the rough-to-smooth layer, in which the local equilibrium approximation is invalid, there is no single dominant velocity scale, in spite of which, the log law (figure 2) still appears to hold.

Figure 20(*a*) suggests that the inertial structures associated with ejections are the true universal motion of the inner layer that scales on y and u_τ or $(-\overline{uv})^{\frac{1}{2}}$ (or $(-\overline{uv}^{-})^{\frac{1}{2}}$) and that therefore this motion does not contribute to the inactive motion nearer to

the wall. Furthermore, at $y/\delta \simeq 0.2$, $L^-_{\tau uv}$ begins to decrease as y increases. Outer layer ejections are growing rapidly owing to the effects of advection, and the loss in correlation with the wall shear stress implies that they have become 'detached'. The division of eddies into attached and 'detached' or freely moving ones is also suggested by the zonal analysis of Fung *et al.* (1991) applied to the DNS database for the low-Reynolds-number channel flow of Kim *et al.* (1987). Thus, assuming that inactive motion is only caused by 'detached' eddies with 'centres' further from the wall than the point under consideration implies that Townsend's (1976, p. 154) equations:

$$\left.\begin{aligned} \frac{\overline{u^2}}{u_\tau^2} &= C_1 - D_1 \log\frac{y}{\delta} \\ \frac{\overline{w^2}}{u_\tau^2} &= C_2 - D_2 \log\frac{y}{\delta} \end{aligned}\right\} \tag{5.2}$$

should be modified so that the log terms (attributed to the inactive motion from attached eddies) include geometry-dependent functions of y/δ and u_τ. Spalart (1988) reaches a similar conclusion. This analysis is consistent with the replacement of Townsend's double-cone eddy (whose diameter scales on y) with a hairpin vortex whose diameter scales on ν/u_τ and is proportional to η and therefore to $y^{\frac{1}{4}}$.

Bradshaw (1967*b*) showed that the energy balance for the inactive motion in the inner layer can be written as:

$$\text{advection} = \text{diffusion} + \text{dissipation}. \tag{5.3}$$

The results of §3.1 show that the turbulent diffusion term, $\partial/\partial y\ (\frac{1}{2}\overline{q^2 v})$ for the inactive motion is small: the pressure–diffusion term is discussed by Morrison *et al.* (1992). Ejections diffuse energy from the inner to the outer layer and provide the local source of inactive motion. Since advection is small near the wall, the main loss of turbulent energy is the outer-layer advection. Additionally, low-wavenumber energy is transported back to the wall by the large-scale inertial eddies associated with sweeps (usually referred to as 'splats') which cause extra direct dissipation in the sublayer. Bradshaw showed that this extra dissipation (in addition to the near-wall advection) is very small so that the inactive energy transported by splats, of which sweeps are a part, is also small. There are therefore two, related sources of inactive motion, both principally caused by splats. The first is low-wavenumber velocity fluctuations in the inner layer, caused by these large eddies, and to a lesser extent by the rest of the outer-layer motion. Splats also cause values of event-averaged fluctuations of u_τ to increase sharply in the inner layer (Morrison & Bradshaw 1989). The second is pressure fluctuations at $y^* < 30$ caused by the splatting mechanism (Moin & Kim 1982) in which splats form pockets in and just above the sublayer, and by which v-component energy is transferred to the two horizontal components. The ϕ_{22} pressure–strain tensor becomes negative at about $y^* = 20$, implying loss of energy from the v-component (Moin & Kim 1985; Mansour, Kim & Moin 1988), while static pressure fluctuations reach a maximum there (Spalart 1988).

The weakness of (4.1) as an estimate of κ is obviously that the denominator of the right-hand side is apparently threshold-dependent although we have not checked this for small changes in threshold about the one used. However, to reiterate, Chen & Bradshaw (1990) recommended a threshold very close to the one used in the present work. Contraction of (4.1), (4.3) and (4.4) provides a more concise definition of κ. Summation of ejection and sweep contributions in these equations gives

$$\left[\frac{-\widetilde{uv}}{-\overline{uv}}\right]^{-\frac{3}{2}} = \kappa\gamma, \tag{5.4}$$

$$\left[\frac{\widetilde{a_1}}{a_1}\right]^{-\frac{3}{2}} = \kappa, \tag{5.5}$$

$$\left[\frac{\widetilde{q^2}}{\overline{q^2}}\right]^{-\frac{3}{2}} = \gamma, \tag{5.6}$$

respectively. $\overline{\tilde{a}_1}$ is the value of a_1 for ejections and sweeps combined. Equations (5.5) and (5.6) are not suitable for the estimation of κ and γ since values of $\tilde{a}_1$ and $\tilde{q}^2$ are made inaccurate by event-averaged values of $\overline{u^2}$ that are 'contaminated' with inactive motion, i.e. u-component motion mis-selected by the scheme as shear-stress bearing. Besides which, there is no objective way of estimating a_1 and $\overline{q^2}$ (for the active motion only). In the log region, the total shear stress, $T \simeq -\rho\overline{uv}$ and $\partial T^*/\partial y^* < 0$ but $\partial T^*/\partial y^* \to 0$ as $Re_\theta \to \infty$, where '*' denotes non-dimensionalization with T_w. Thus $-\overline{uv}^*$ increases and tends to unity as $Re_\theta \to \infty$. (Huffman & Bradshaw (1972) explained any apparent variation in κ with Reynolds number as a change in the additive constant in the log law caused by non-zero $\partial T^*/\partial y^*$.) Similarly, as the Reynolds number increases, the influence of sources or sinks in a first-order inertial subrange diminishes and, in the limit, the spectral transfer of energy equals the dissipation. In other words, $-\overline{uv}^*$ can also be expected to increase. The present results are therefore not especially helpful in determining whether κ is Reynolds-number dependent or not. However, they do suggest that it is the universal spectral flux that determines κ and that violations of the local equilibrium approximation will cause κ to change, as (2.3) might suggest. Spalart's (1988) simulation data obey the local equilibrium approximation accurately for $y^* > 40$. Thus

$$\epsilon^* = -\overline{uv}^* \partial U^*/\partial y^* = 1/\kappa y^*$$

is universal and therefore so is κ at constant y^*. Note that (5.4) is independent of non-universal forms of spectral flux (see Lumley 1964).

In §2, we introduced the concept of a first-order inertial subrange, for which a sufficient condition is that energy sources and sinks in the range are a small fraction of the spectral energy transfer. If this range coincides with a local equilibrium region at sufficiently high Reynolds numbers ($Re_\lambda > 100$), then the small effect of sources or sinks in wavenumber space can be attributed to the small spatial transport of energy. The collapse of the conditionally averaged triple products for, say, sweeps on $(-\overline{uv}^+)^{\frac{3}{2}}$ and $(-\overline{uv})^{\frac{3}{2}}/\gamma^+$ in the log region, and the fact that the spatial energy transport is small there suggests that ejections and sweeps effect virtually all the universal part of the spectral energy transfer, ejection and sweep lengths in the smooth-wall log region (figure 7*a*) corresponding approximately with wavenumbers near the middle of the first-order inertial subrange. Thus, (3.6) and (5.4) define κ. Coincidence of a first-order inertial subrange with local equilibrium implies that this definition has an analogue in physical space: this is given by (4.3) and (5.5) and arises because $L_\epsilon = L_\epsilon^+ = L_\epsilon^-$.

Although the results neither confirm nor deny any non-universal behaviour in κ, they do show that it really depends on the universal part of the spectral energy transfer (equation (5.4)) or equivalently derives from the local equilibrium approximation (equation (5.5)). Since application of wall scaling to the complete

energy equation leads to the local equilibrium approximation, it may equally be supposed (as is perhaps more common the case) that κ is the constant appearing in the dimensional analysis for the log region, $y^* > 30$, $y/\delta < 0.2$.

6. Conclusions

Event-averaged statistics from the uv-based sampling scheme, in particular event lengths and triple products suggest that ejections and sweeps in the log region are responsible for virtually all the universal part of spectral energy transfer. Moreover, the energy transfer appears to be localized in physical space in the form of Falco's typical eddies and also in wavenumber space in the form of a first-order inertial subrange, for which a sufficient criterion is only that local sources and sinks are a small fraction of the inertial transfer. If the inner-layer motion consisted entirely of ejections and sweeps, the dissipation lengthscale, L_τ, for the universal motion would be equal to y and not to κy.

The inertial eddy of which an ejection is the 'centre' gives correlation lengthscales that are directly proportional to y and is therefore the true universal motion of the inner layer and corresponds to Townsend's attached eddy. Once in the outer layer, ejections appear to become 'detached' and to effect most of the outer layer diffusion of energy. Thus it is principally ejections that control the interaction of the inner and outer layers (as Kline *et al.* originally suggested), and therefore the value of u_τ. All the evidence suggests that there is strong correspondence between visually observed bursts and attached eddies (as detected here), and we therefore regard them as synonymous.

Sweeps appear to be inverted typical eddies moving back down towards the wall and are mirror images of ejections about the line joining the two centres of vorticity. Outer-layer sweeps are the near-universal constituent of the motion where, if the motion as a whole were in equilibrium and consisted purely of sweeps, the appropriate dissipation lengthscale would equal δ. Although sweeps are part of the universal motion in the inner layer, the associated large eddy, a splat, which is 'detached' and scales on δ and u_τ, induces inactive motion. This takes two forms: the low-wavenumber velocity fluctuations that are superimposed on the universal higher-wavenumber motion and, as the eddy approaches the wall, pressure fluctuations produced by the splatting mechanism at $y^* = 20$–30. Inactive motion is also shown to be dependent on the distance from the wall, even in the logarithmic region.

The present work demonstrates the importance of a first-order inertial subrange (a wavenumber-domain equivalent of the local equilibrium approximation): in particular, κ is shown to depend on the universal part of the spectral flux and this quantity rather than deductions from a Clauser plot is more likely to show any non-universal behaviour in κ. An important implication of these results is that the universal spectral transfer is localized in wavenumber space (even at the relatively high Reynolds numbers of these experiments) and is described by the simple constitutive relations, equations (5.4)–(5.6) which can be used as the basis of a sub-grid scale model for large-eddy simulations. These relations explain the success of several workers in being able to obtain apparently good results with a cut-off in the first-order inertial subrange without the need for a true inertial subrange with local isotropy (Ferziger 1977). The same comments apply to 'split-spectrum' modelling techniques in Reynolds-averaged calculations.

We are grateful to the Editor and referees for their helpful comments. We are also indebted to the United States Army and the Science and Engineering Research Council (Grant GR/C/56856) for financial support.

REFERENCES

ANDREOPOULOS, J. 1978 Symmetric and asymmetric near wake of a flat plate. PhD thesis, Imperial College, London.

ANTONIA, R. A. & LUXTON, R. E. 1972 The response of a turbulent boundary layer to a step change in surface roughness. Part 2. Rough-to-smooth. *J. Fluid Mech.* **53**, 737.

BRADSHAW, P. 1967*a* The turbulence structure of equilibrium turbulent boundary layers. *J. Fluid Mech.* **29**, 625.

BRADSHAW, P. 1967*b* 'Inactive' motion and pressure fluctuations in turbulent boundary layers. *J. Fluid Mech.* **30**, 241.

BRADSHAW, P. 1967*c* Conditions for the existence of an inertial subrange in turbulent flow. *Natl Phys. Lab. Aero. Rep. No.* 1220.

BRADSHAW, P., FERRISS, D. H. & ATWELL, N. P. 1967 Calculation of boundary-layer development using the turbulent energy equation. *J. Fluid Mech.* **28**, 593.

CHEN, M. Z. & BRADSHAW, P. 1990 Studies of burst-detection schemes by use of direct simulation data for fully-turbulent channel flow. Unpublished report.

CHU, C. C. & FALCO, R. E. 1988 Vortex ring/viscous wall layer interaction model of the turbulence production process near walls. *Exps. Fluids* **6**, 305.

CLAUSER, F. H. 1956 The turbulent boundary layer. *Adv. Appl. Mech.* **4**, 1.

COLES, D. E. 1955 The law of the wall in turbulent shear flow. In *50 Jahre Grenzschichtforschung* (ed. H. Gortler & W. Tollmien), pp. 153–163. Braunschweig: F. Vieweg.

COLES, D. E. 1956 The law of the wake in the turbulent boundary layer. *J. Fluid Mech.* **1**, 191.

COLES, D. E. 1962 The turbulent boundary layer in a compressible fluid. Appendix A: A manual of experimental boundary-layer practice for low-speed flow. *Rand Corporation Rep.* R-403-PR.

COLES, D. E. & HIRST, E. A. (ed.) 1969 *Proc. 1968 AFOSR-IFP-Stanford Conference on Computation of Turbulent Boundary Layers.* Thermosciences Division, Stanford University.

CORINO, E. R. & BRODKEY, R. S. 1969 A visual observation of the wall region in turbulent flow. *J. Fluid Mech.* **37**, 1.

DOMARADZKI, J. A. & ROGALLO, R. S. 1990 Local energy transfer and nonlocal interactions in homogeneous, isotropic turbulence. *Phys. Fluids* A **2**, 413.

FALCO, R. E. 1974 Some comments on turbulent boundary layer structure inferred from the movements of a passive contaminant. *AIAA paper* 74-99.

FALCO, R. E. 1977 Coherent motions in the outer region of turbulent boundary layers. *Phys. Fluids Suppl.* **20**, S124.

FALCO, R. E. 1979 Structural aspects of turbulence in boundary layer flows. *Proc. Sixth Biennial Symposium on Turbulence.* Rolla Missouri.

FALCO, R. E. 1980 The production of turbulence near a wall. *AIAA paper* 80-1356.

FALCO, R. E. 1983 New results, a review and synthesis of the mechanism of turbulence production in boundary layers and its modification. *AIAA paper* 83-0377.

FALCO, R. E. 1984 Recent progress in understanding the turbulence production process. *Michigan State Univ. Dept Mech. Engng Rep.* TSL-84-1.

FALCO, R. E., KLEWICKI, J. C., PAN, K. & GENDRICH, C. P. 1989 Production of turbulence in boundary layers. *Proc. 7th Symp. on Turbulent Shear Flows, Stanford University*, paper 2–5.

FERZIGER, J. H. 1977 Numerical simulations of turbulent flows. *AIAA J.* **15**, 1261.

FUNG, J. C. H., HUNT, J. C. R., PERKINS, R. J., WRAY, A. A. & STRETCH, D. 1991 Defining the zonal structure of turbulence using the pressure and invariants of the deformation tensor. *Advances in Turbulence 3*, (ed. A. V. Johansson & P. H. Alfredsson), pp. 395–404.

GUENZENNEC, Y. G., PIOMELLI, U. & KIM, J. 1987 Conditionally-averaged structures in wall-bounded turbulent flows. In *Studying Turbulence Using Numerical Simulation Databases.* Ames/Stanford CTR-587, p. 263.

HEAD, M. R. & BANDYOPADHYAY, P. 1981 New aspects of turbulent boundary-layer structure. *J. Fluid Mech.* **107**, 297.

HUFFMAN, G. D. & BRADSHAW, P. 1972 A note on von Kármán's constant in low Reynolds number turbulent flows. *J. Fluid Mech.* **53**, 45.

HUNT, J. C. R. 1988 Studying turbulence using direct numerical simulation: 1987 Center for Turbulence Research NASA Ames/Stanford Summer Programme. *J. Fluid Mech.* **190**, 375.

KIM, H. T., KLINE, S. J. & REYNOLDS, W. C. 1971 The production of turbulence near a smooth wall in a turbulent boundary layer. *J. Fluid Mech.* **50**, 133.

KIM, J. 1985 Evolution of a vortical structure associated with the bursting event in a channel flow. *Proc. 5th Symp. on Turbulent Shear Flows*, Cornell University.

KIM, J. & MOIN, P. 1986 The structure of the vorticity field in turbulent channel flow. Part 2. Study of ensemble-averaged fields. *J. Fluid Mech.* **162**, 339.

KIM, J., MOIN, P. & MOSER, R. D. 1987 Turbulence statistics in fully developed channel flow at low Reynolds number. *J. Fluid Mech.* **177**, 133.

KLEBANOFF, P. S. 1954 Characteristics of turbulence in a boundary layer with zero pressure gradient. *NACA Tech. Note* 3178.

KLINE, S. J., REYNOLDS, W. C., SCHRAUB, F. A. & RUNSTADLER, P. W. 1967 The structure of turbulent boundary layers. *J. Fluid Mech.* **30**, 741.

KOVASZNAY, L. S. G., KIBENS, V. & BLACKWELDER, R. F. 1970 Large scale motions in the intermittent region of a turbulent boundary layer. *J. Fluid Mech.* **41**, 283.

LIGRANI, P. M. 1989 Structure of turbulent boundary layers. *Encyclopedia of Fluid Mechanics* (ed. N. P. Cheremisinoff), ch. 5. Gulf.

LUMLEY, J. L. 1964 Spectral energy budget in wall turbulence. *Phys. Fluids* **7**, 190.

MANSOUR, N. N., KIM, J. & MOIN, P. 1988 Reynolds-stress and dissipation-rate budgets in a turbulent channel flow. *J. Fluid Mech.* **194**, 15.

MESTAYER, P. 1982 Local isotropy and anisotropy in a high-Reynolds-number turbulent boundary layer. *J. Fluid Mech.* **125**, 475.

MOIN, P. & KIM, J. 1982 Numerical investigation of turbulent channel flow. *J. Fluid Mech.* **118**, 341.

MOIN, P. & KIM, J. 1985 The structure of the vorticity field in turbulent channel flow. Part 1. Analysis of instantaneous fields and statistical correlations. *J. Fluid Mech.* **155**, 441.

MOIN, P., LEONARD, A. & KIM, J. 1986 Evolution of a curved vortex filament into a vortex ring. *Phys. Fluids* **29**, 955.

MORRISON, J. F. & BRADSHAW, P. 1989 Bursts and wall shear stress fluctuations in turbulent boundary layers. *Proc. 7th Symp. on Turbulent Shear Flows, Stanford University*, paper 2-2.

MORRISON, J. F. & BRADSHAW, P. 1992 The thermal boundary layer downstream of a rough-to-smooth change in surface roughness. Report in preparation.

MORRISON, J. F., SUBRAMANIAN, C. S. & BRADSHAW, P. 1992 Bursts and pressure fluctuations in turbulent boundary layers. Report in preparation.

MORRISON, J. F., TSAI, H. M. & BRADSHAW, P. 1986 Conditional-sampling schemes based on the Variable-Interval Time-Averaging (VITA) algorithm. *Imperial College Aero. Rep.* 86-01.

MORRISON, J. F., TSAI, H. M. & BRADSHAW, P. 1989 Conditional-sampling schemes for turbulent flow, based on the Variable-Interval Time-Averaging (VITA) algorithm. *Exps Fluids* **7**, 173.

MURLIS, J., TSAI, H. M. & BRADSHAW, P. 1982 The structure of turbulent boundary layers at low Reynolds number. *J. Fluid Mech.* **122**, 13.

OFFEN, G. R. & KLINE, S. J. 1974 Combined dye-streak and hydrogen-bubble visual observations of a turbulent boundary layer. *J. Fluid Mech.* **62**, 223.

OFFEN, G. R. & KLINE, S. J. 1975 A proposed model of the bursting process in turbulent boundary layers. *J. Fluid Mech.* **70**, 209.

ROBINSON, S. K. 1990 The kinematics of turbulent boundary layer structure. PhD thesis, Stanford University, and *NASA TM* 103859.

ROBINSON, S. K. 1991 Coherent motions in the turbulent boundary layer. *Ann. Rev. Fluid Mech.* **213**, 601.

ROGERS, M. M. & MOIN, P. 1987 The structure of the vorticity field in homogeneous turbulent flows. *J. Fluid Mech.* **176**, 33.

SADDOUGHI, S. D., VEERAVALLI, S. V., PRASKOVSKY, A. A. & BRADSHAW, P. 1991 Paper presented at APS Fluid Dyn. Div. Ann. Mtng.

SCHOFIELD, W. H. 1981 Turbulent shear flows over a step change in surface roughness. *Trans. ASME* I: *J. Fluids Engng* **103**, 344.

SPALART, P. R. 1988 Direct simulation of a turbulent boundary layer up to $R = 1410$. *J. Fluid Mech.* **187**, 61.

SUBRAMANIAN, C. S., KANDOLA, B. S. & BRADSHAW, P. 1985 Measurements of the low-wave-number structure of a turbulent boundary layer. *Imperial College Aero. Rep.* 85-01.

TENNEKES, H. & LUMLEY, J. L. 1972 *A First Course in Turbulence.* MIT Press.

THEODORSEN, T. 1952 Mechanism of turbulence. In *Proc. 2nd Midwestern Conf. on Fluid Mechanics, Ohio State University*, p. 1.

TOWNSEND, A. A. 1961 Equilibrium layers and wall turbulence. *J. Fluid Mech.* **11**, 97.

TOWNSEND, A. A. 1966 The flow in a turbulent boundary layer after a change in surface roughness. *J. Fluid Mech.* **26**, 255.

TOWNSEND, A. A. 1976 *The Structure of Turbulent Shear Flow*, 2nd edn. Cambridge University Press.

TRITTON, D. J. 1967 Some new correlation measurements in a turbulent boundary layer. *J. Fluid Mech.* **28**, 341.

WILLMARTH, W. W. & TU, B. J. 1967 Structure of turbulence in the boundary layer near the wall. *Phys. Fluids Suppl.* **10**, S134.

YEUNG, P. K. & BRASSEUR, J. G. 1991 The response of isotropic turbulence to isotropic and anisotropic forcing at the large scales. *Phys. Fluids* A **3**, 884.